WYLE LABORATORIES - RESEARCH STAFF

REPORT NUMBER WR 67-8

THEORETICAL AND EXPERIMENTAL RESPONSE OF PANELS TO TURBULENT BOUNDARY LAYER PRESSURE FLUCTUATIONS AND SEPARATED FLOW. ~ SOME PRELIMINARY RESULTS

By

M. J. Crocker

Work Performed Under Contract NAS8-5384

Prepared by M. J. Crocker
M. J. Crocker

Approved by R. C. Kao for R.C.P.
R. C. Potter
Program Manager

Approved by L. C. Sutherland
L. C. Sutherland
Director of Research Staff, Huntsville

Date JUL 1967

COPY NO. 2

SUMMARY

A powerful theoretical method has been developed which predicts the response of simply-supported panels to turbulent boundary layer pressure fluctuations. This method, in conjunction with the digital computer program presented, can also be used to predict full scale structural response to turbulence, and for this case novel methods have been developed to describe the empirical expressions for the narrow band wall pressure space correlations, necessary for the computations. Experimental success has also been achieved in setting up repeatable separated flow with small longitudinal wall pressure gradients.

The basic experimental techniques for measuring panel response were developed. Unfortunately, difficulty was experienced in constructing a sufficiently uniform panel. Results for the panel actually used are given, but are thought to be unrepresentative. Recommendations for further tests are put forward.

TABLE OF CONTENTS

TABLE OF CONTENTS (Continued)

LIST OF FIGURES

Figure

LIST OF FIGURES (Continued)

Figure

LIST OF FIGURES (Continued)

Figure

LIST OF SYMBOLS

a	=	length of panel along x-axis
b	=	width of panel along y-axis
c	=	speed of sound in air
C_m	=	bending wave velocity component for m-elastic half waves along the x-axis
C_{mn}	=	generalized damping coefficient for mn mode of panel
E	=	Young's modulus of elasticity
f	=	frequency
$f_{coinc.}$	=	frequency of longitudinal coincidence of panel
f_m	=	resonance frequency of the m-th longitudinal mode of the panel
$f_{mn}(x,y)$	=	normalized mn mode shape of the panel
$F_{mn}(t)$	=	generalized force on panel for mn mode at time t
F_{omn}	=	amplitude of the generalized force $F_{mn}(t)$
h	=	thickness of panel (along z-axis)
$H(\omega/\omega_{omn})$	=	single degree of freedom dynamic magnification factor for mn mode of panel
i	=	$\sqrt{-1}$
I	=	second moment of area of panel $= h^3/12$
$J^2_{mn}(\omega)$	=	joint-acceptance of mn mode of panel at frequency ω
k_{mn}	=	acoustic radiation damping parameter
K_{mn}	=	generalized stiffness of mn mode of panel

LIST OF SYMBOLS (Continued)

m	=	number of elastic half waves of panel in x-direction
$M = M_o$	=	Mach number of free stream flow
M_{mn}	=	generalized mass of mn mode of panel
n	=	number of elastic half waves of panel in y-direction
N	=	number of blades of centrifugal fan
p	=	pressure
p_x, p_y	=	joint-acceptance parameters
$P(x,y,t;\omega)$	=	instantaneous harmonic pressure acting on panel at point x, y, time t, and at frequency ω.
$q_{mn}(t)$	=	generalized modal displacement coordinate for mn mode of panel at time t
$q_{o_{mn}}$	=	amplitude of generalized modal displacement coordinate $q_{mn}(t)$
$\dot{q}_{mn}(t)$	=	generalized modal velocity for mn mode of panel at time t
$\ddot{q}_{mn}(t)$	=	generalized modal acceleration for mn mode of panel at time t
q_x, q_y	=	joint-acceptance parameters
Q_{mn}	=	dynamic magnification factor for mn mode of panel at resonance
$Q_p(\ \ )$	=	double pressure space-time covariance for a homogeneous wall pressure field
r_x, r_y	=	joint-acceptance parameters

LIST OF SYMBOLS (Continued)

R_{mn}	=	frequency parameter for m n mode of a clamped-clamped panel
$R_p(x,y,x',y';\omega)$	=	wall pressure spatial cross-correlation function for points (x,y) and (x', y') at frequency ω
$R_p(\xi, 0, 0;\omega)$	=	longitudinal narrow band space correlation coefficient of wall pressure field at zero time delay and at frequency ω
$R_p(0, \zeta, 0;\omega)$	=	lateral narrow band space correlation coefficient of wall pressure field at zero time delay and at frequency ω
$S_p(\omega)$	=	power spectral density of wall pressure at frequency ω
$S_p(x, y, x', y';\omega)$	=	pressure spatial cross power spectral density for points (x,y) and (x',y') at frequency ω
S_r	=	cross sectional area of duct (or wind-tunnel)
$S_{w_{mn}}(x, y;\omega)$	=	power spectral density of panel displacement for point x, y on panel at frequency ω, for m n mode
$S_w(x, y;\omega)$	=	power spectral density of panel displacement for point x, y on panel at frequency ω, summed over all modes
$S_{\ddot{w}}(x, y;\omega)$	=	power spectral density of panel acceleration for point x, y on panel at frequency ω, summed over all modes.
t	=	time
U_c	=	mean convection velocity of pressure fluctuations in the turbulent boundary layer
$U_o = U_\infty$	=	free stream velocity of pressure fluctuations in the turbulent boundary layer
U (x, y, t)	=	total displacement of point (x,y) on panel at time t (summed over all panel modes)

$w_{mn}(x, y, t; \omega)$	=	instantaneous displacement at a point (x,y) on panel at time t in mn mode at frequency ω
x	=	longitudinal panel coordinate axis (in flow direction)
$\bar{x}$	=	non-dimensional form of $x = x/a$
y	=	lateral panel coordinate axis (perpendicular to flow axis, in plane of panel)
$\bar{y}$	=	non-dimensional form of $y = y/b$
z	=	coordinate axis perpendicular to plane of panel
z	=	depth of separated flow section

Greek Symbols

α	=	frequency parameter for a clamped-clamped panel
α	=	phase angle of cross spectral density ($= -\omega \xi/U_c$)
$\beta(\omega/\omega_o)$	=	phase angle between force and displacement
γ	=	frequency parameter for a clamped-clamped panel
γ_x	=	longitudinal wall pressure correlation length parameter
γ_y	=	lateral wall pressure correlation length parameter
δ	=	boundary layer thickness
δ^*	=	boundary layer displacement thickness
δ_{mn}	=	critical damping ratio for the mn mode of the panel equals $1/(2\phi_{mn})$
$\delta_{r_{mn}}$	=	acoustic radiation critical damping ratio for mn mode of panel
δ_x	=	longitudinal wall pressure space correlation decay rate

LIST OF SYMBOLS (Continued)

δ_y	=	lateral wall pressure space correlation decay rate
Δ_x, Δ_y	=	joint-acceptance parameters
ζ	=	lateral separation distance = $y - y'$
$\bar{\zeta}$	=	non-dimensional form of $\zeta = \zeta/b$
λ	=	eddy wavelength
λ_m	=	bending wavelength of the m-th longitudinal mode of panel
μ	=	surface density of panel = ρh
ν	=	Poisson's ratio
ξ	=	longitudinal separation distance = $x - x'$
$\bar{\xi}$	=	non-dimensional form of $\xi = \xi/a$
ξ_{mn}	=	generalized mass fraction for m n mode of panel
ρ	=	panel density
ρ_o	=	density of air
τ	=	time delay between two measured signals
Φ_p ( )	=	cross spectral density of wall pressure fluctuations
Φ_x	=	factor for longitudinal component of turbulence joint-acceptance
Φ_y	=	factor for lateral component of turbulence joint-acceptance
ψ	=	frequency parameter for a clamped-clamped panel
ω	=	angular frequency = $2\pi f$

$\omega_{o_{mn}} = \omega_{mn}$	=	undamped angular resonance frequency of mn mode of panel
Ω	=	rotational speed of fan r.p.m.

Other Notations

$\lvert\ \rvert$	denotes absolute value
$\overline{\qquad}$	denotes time average.

1.0 INTRODUCTION

As a typical space vehicle ascends through the atmosphere it is subjected to severe fluctuating surface pressures which act as the major source of excitation for structural vibrations of the vehicle (Reference 1). Except for the first ten or twenty seconds of flight, when the exhaust noise predominates, the dominant source of unsteady pressure loading on the vehicle is due to pressure fluctuations in the turbulent boundary layer of the flow. This turbulent boundary layer is mostly attached to the vehicle but in some regions, in the vicinity of flares and steps, the flow is separated. Other sources of fluctuating loads are due to oscillating shocks and wake and base pressure fluctuations. These other sources often interact or couple with the turbulent boundary layer flow; however, an estimate of structural response, at least to a first order, can most easily be made by neglecting such interaction and coupling. The total structural response can finally be estimated by summing the responses to each source of loading.

Work is available on experimental and theoretical studies of panel response to attached boundary layer flow pressure fluctuations (References 3, 4, and 5; also see Bibliography, Appendix B). However, in general the agreement between theory and experiment is not too good and is more qualitative than quantitative in nature. It appears at present that no theoretical or experimental work has been published on panel response due to pressure fluctuations caused by separated turbulent boundary layers. Separated supersonic flows are usually accompanied by oscillating shocks. However the response of panels to sinusoidally oscillating shocks has been analyzed in detail in Reference 2 and therefore is not considered in this report.

The purpose of the work described here is to compare theoretically predicted panel response to boundary layer pressure fluctuations with panel response measured in a carefully controlled experiment. The intention is to initially confine the experiment to attached turbulent boundary layers and then extend it to cover the case of separated turbulent boundary layer flow. The total program of work has not been completed and some of the experimental results measured are unsatisfactory; however, considerable success has been achieved with the theoretical prediction of panel response. Thus, it is felt valuable at this time to present a review of the work to date indicating what has been achieved in the program both experimentally and theoretically and also where improvement can be made in the theory and experiments to bring the program to a satisfactory conclusion.

In Section 2 of this report, details of the aerodynamic measurements of separated flow and of turbulent boundary layer pressure fluctuations, as well as structural measurements of panel response to acoustic waves and to turbulence, are given. In Section 3 of this report, theory is developed which predicts panel response to turbulent boundary layer pressure fluctuations; discussion is also given as to the parameters of the pressure field which must be determined for the theoretical

calculations. In Section 4, the theoretical computations of panel response using the theory given in Section 3 and the computer program given in Appendix A are discussed. The report is concluded with a Bibliography in Appendix B and a discussion of the acoustic damping problem of a panel mounted in the wall of a wind tunnel, in Appendix C.

2.0 EXPERIMENTAL APPARATUS AND PROCEDURE

2.1 General Discussion

The experimental measurements were made with the use of Wyle Laboratories' Low Speed Wind Tunnel. This tunnel is capable of operating at speeds of up to 150 fps with a rectangular working section of 10 in. by 32 in. The tunnel is powered by a 12 blade centrifugal fan mounted at the tunnel exit, and has a bell mouth intake with a honeycomb to reduce free-stream turbulence. It was designed to be a low noise tunnel in that the section of the tunnel, downstream of the working section, as far as the expansion before the fan, was lined with foam rubber to absorb compressor noise. A view of the working section of the wind tunnel, which was constructed from masonite and plexiglass, is given in Figure 1.

The measurements made in the tunnel can be divided into aerodynamic, and structural response measurements and are discussed in the following two sections of the report, respectively.

The aerodynamic measurements consisted firstly of mean velocity profiles and wall static pressure patterns measured in the separated flow which was established in the special adjustable section, constructed especially for the task. These measurements were necessary, since mean separated flow measurements are sparse, unlike similar attached flow measurements, and the response of a panel will depend upon the parameters of the separated flow to which it is subjected. Secondly the aerodynamic measurements included the overall level and frequency spectrum of the wall pressure fluctuations for both the attached and separated turbulent boundary layer flow. The other statistical properties of attached boundary layer flow which must be known before panel response can be computed, namely the spatial narrow-band wall pressure correlations and the turbulence convection velocity were not measured, since these have been extensively studied by other workers (References 3, 5, and 6) and are discussed in Section 3.1.1 of this report. However, this is not the case for separated flow, and before panel response can be calculated theoretically for a separated turbulent boundary layer it will be necessary to measure the longitudinal and lateral narrow-band spatial wall pressure correlations and the velocity of convection of the turbulence in the flow. These measurements have not yet been completed.

The structural response measurements include measurements of the panel response to grazing incidence and to normal incidence acoustic waves in order to determine the resonance frequencies of the panel. Also the measurements covered the panel response to attached turbulent boundary layer flow. Panel response to separated turbulent boundary layer flow has yet to be measured.

The aerodynamic and structural measurements are now discussed in some detail in the following Sections, 2.2, and 2.3.

2.2 Aerodynamic Considerations

2.2.1 Aerodynamic Measurements of Separated Turbulent Boundary Layer Flow*

The structure of the separated flow was first measured by using special adjustable separated flow section shown in Figures 1 and 2. It was possible to adjust the depth of the floor of the section, the angle of the floor to the horizonal and also the height of the step at the rear of the section. At the beginning of the section a small aluminum flap was fitted, as shown in Figure 1.

Before each set of wall static pressure readings was taken, the separated flow section was sealed off with tape as shown in Figure 2. The whole underside of the separated flow section was covered by a pressure equalization box which was vented to the tunnel static pressure, about 18 inches downstream of the rear of the section, by a series of holes cut in the flexible aluminum floor at this point in the tunnel. The purpose of this pressure equalization box was to eliminate a static pressure differential across the panel whose response was being measured, and also to reduce the severe loads imposed on the adjustable parts of the separated flow section.

A series of static pressure holes were drilled in the floor of the separated flow section, and connected to a multi-tube manometer as shown in Figure 1. Initially the floor of the section was kept horizontal and the rear step adjusted so that the cross-sectional area before and after the separated flow section was the same. With the floor height as the variable, a series of measurements of the floor static pressure were made by photographing the fluid levels in the tubes of the manometer (which was tilted to 25 degrees from the horizontal). Mean curves drawn through these readings are presented in Figures 3 and 4.

These readings suggested two types of separation. For small separated flow floor depths (z) (see Figure 3) there was an appreciable pressure rise at separation and a large pressure drop at the reattachment step. However, as the separated flow floor depth (z) was increased (see Figure 4) the pressure rise at separation was reduced and eventually became a small pressure drop; and the pressure drop at reattachment persisted although it was reduced in magnitude.

The configuration with $z = 3\ 1/2$ in. (see Figure 4) was chosen for further study since this configuration exhibited almost zero pressure gradient ($\partial p/\partial x$), over most

---

* Measurements reported in Section 2.2.1 were performed under contract NAS8-11308, and are included here because of their relevance to the overall study.

of the separated flow section floor, (at least where it was planned to place the panel under investigation). The choice of this configuration was made for two reasons: first it removed a variable ($\partial p/\partial x$) in the study of the separated flow itself, and second it removed the necessity of having a non-uniform static load over the panel.

It was found that if a small protuberance of about 0.1 in. height was positioned at the beginning of the separated flow section as shown in Figure 5, the static pressure pattern was changed considerably for the same depth, z. The pressure pattern with this step is shown in Figure 5 for z = 3 1/2 in. This may be compared with Run 7 of Figure 4. It is seen that there is now a pressure drop at separation and a much reduced pressure drop at reattachment. The static pressure between these two points is also lower, although the general shape is maintained. It is interesting to note that such a protuberance also changed the velocity of the reversed flow (this is discussed below).

Measurements of the velocity profile at five stations (see Figure 3) in the separated flow were made with a United Sensor Probe, Type x - 125, for z = 3 1/2 in. This pitot-static probe is sensitive to both pitch and yaw and is shown in the upper part of Figure 2. Three of the five traverses carried out are given in Figure 6. The traverses (which were made with no initial protuberance present) indicate that the reverse flow increases from about 20 fps at the beginning of the separated flow section to about 50 fps at the rear of the section. The rate of shear is seen to decrease from the front to the rear of the separated flow section and the mixing region likewise becomes thicker in the same direction. In fact the flow is reminiscent of the mixing flow from a slot jet. Figures 7 and 8 show the velocity profiles of the reverse flow at Station 5 (see Figure 3) measured with the Boundary Layer Pitot Tube shown in the lower part of Figure 2. This pitot tube was constructed from hypodermic tubing which was flattened to an outer dimension of 0.025 in., and an inner dimension of about 0.008 in. In Figure 7, the velocity profiles (with and without an initial protuberance at the beginning of the separated flow section) are shown for the flow immediately next to the floor of the section. The flow was traversed from the floor to point 5 approximately one inch away from the floor. It is interesting to notice that the effect of the protuberance is to considerably increase the velocity of the reverse flow. Figure 8 shows the same velocity profiles for the first one inch from the floor and thus show the reversed flow floor boundary layer.

2.2.2 Measurements of Wall Pressure Fluctuations for Attached and Separated Turbulent Boundary Layer Flow

A 1/4 in. condenser microphone was flush-mounted in the center of the floor of the separated flow working section. The boundary layer pressure fluctuations were measured first with the separated flow section floor in the flush position, so that the flow was not separated and was a simple turbulent boundary layer flow. Figure 9 shows the power spectrum of the pressure fluctuations in one third octave bands.

Figure 10 shows the spectral density of the pressure fluctuations (measured with a 2 Hz. bandwidth filter and a total sweep time of 60 minutes).

In Figures 11 and 12, the power spectrum in one third octave band levels and the spectral density of the pressure fluctuations (measured in the same way as above) are presented, respectively, for separated flow with the separated flow floor depth (z) equal to 3 1/2 inches.

It is observed that in Figures 9 and 10 the curves are not smooth and that there appears to be a large low frequency content to the flow and also "discrete" frequency peaks at 21, 37, and 59 Hz. This is not typical of a normal turbulent boundary layer pressure spectrum and the discrete peaks at first might be suspected to be produced by the centrifugal fan. However, for a fan the fundamental tone f is given by:

$$f = \frac{N\,\Omega}{60} \quad \text{Hz.} \tag{1}$$

where N is the number of blades,

Ω is the rotational speed in r.p.m.

For the tests described in this report, the fan was always run at high speed, i.e., Ω = 1305, (21.75 Hz.) and was 12 bladed, i.e., N = 12.

Thus $$f = 1305 \times \frac{12}{60} = 261 \text{ Hz.}$$

It is seen that this fundamental frequency is much greater than discrete frequencies observed in Figures 9 and 10.

The frequency peak at 59 Hz. is probably due to the main power supply, and that at 37 Hz. is coincident with the fundamental tone of Wyle main compressor facility. The peak at 21 Hz. is at the rotational frequency of the wind tunnel blower. Thus it appears that all frequency peaks observable in Figures 9 and 10 can be disregarded.

The pressure spectrum presented in Figures 11 and 12 for the separated flow is relatively smooth and typical, exhibiting only one small peak at about 23 Hz.- presumably again the fan rotational frequency.

Measurements, made by other investigators, of the longitudinal and lateral spatial pressure correlations and of the convection velocity for the attached boundary layer case will suffice, however; for the case of the separated boundary layer, such work still needs to be carried out, since it is unavailable in the literature.

2.3 Panel Response

A panel mount was machined from a rectangular piece of aluminum measuring 18 1/2 in. by 32 in. by 3/8 in thick. The panel mount was stiffened by the addition on its undersurface of four 1 inch angle sections. A 1/2 inch layer of "Vibrodamper" damping compound was also applied to the undersurface of the mount to further reduce vibration.

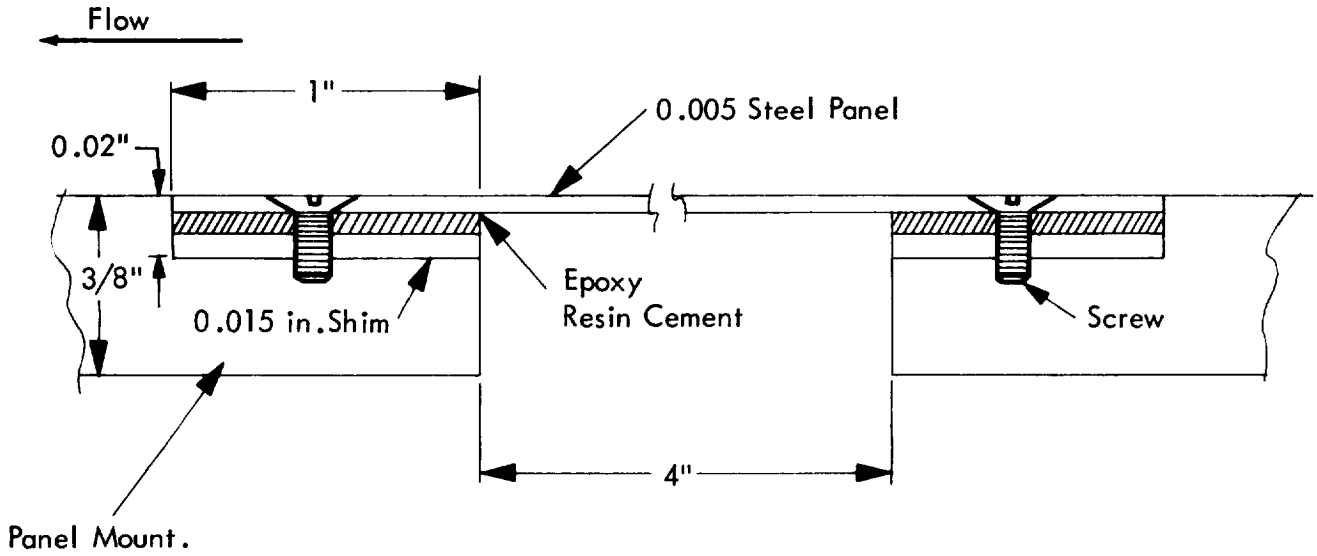

A 4 inch by 8 inch hole was cut in the panel mount, as shown in Figures 13 and 14. Bordering this hole a 0.020 inch recess of 1 inch width was cut into the panel mount. By using appropriate thickness shims, 6 inch by 10 inch pieces of metal could be let in to this recess, producing effective panels, 4 inch by 8 inch as shown in the above sketch. The steel panels were glued in position with epoxy resin cement and, finally, to guard against catastropic failure, held in place with a few small screws. It was intended that this method of fixture would closely simulate fully-fixed edge conditions. Several non-uniformities were observed in the panels which had a tendency to "oil-can". Several panels were constructed in an attempt to correct this fault, both 0.02 inch aluminum and 0.005 inch steel panels being tried. Although later panels were improvements over the initial efforts, surface wrinkling was still observable and "oil-canning" still occurred. The results given in this report were eventually taken on the 0.005 inch steel, in spite of its faults, as this was, at the time, the best available.

The vibration of the panel support, originally thought to be a problem, was reduced by making it massively stiffer and treating it with "Vibrodamper" damping compound. The fundamental resonance frequency for an unstiffened sheet of aluminum with the

dimensions of the support (18.5 in. by 32.0 in. by 0.375 in.) calculates from Equation (2) to be $\approx$ 134 Hz. The stiffened support would have a higher fundamental frequency.

2.3.1 Panel Response to Acoustic Waves Generated by a Loudspeaker

The response of a 0.005 in. thich steel panel to acoustic waves arriving at both normal and grazing incidence was measured. Figure 14 shows the apparatus for a normal incidence test. Figures 15 and 16 show block diagrams of the electronic apparatus used. The purpose of the tests was to determine the resonant frequencies of the panel for comparison with theoretical predictions and with the response measured to boundary layer excitation.

Figure 17 and 18 show typical displacement/frequency curves obtained using the apparatus of Figure 15 for normal and grazing incidence acoustic excitation respectively. The Photocon PT-5 displacement transducer was positioned 0.010 in. away from the quiescent panel to obtain these results. A static calibration (adjusting the distance of the pick-up from the panel) showed that the instrument was linear over $\pm$ 0.002 in.; the displacement was thus limited to this range. This in turn dictated an SPL of approximately 89 dB for the test setup, (see Figure 14) which level was maintained constant over the range of 30 to 1,000 Hz. (by use of a compressor system). No measurements were possible below 30 Hz., due to the inability of the speaker system to produce sine waves below this frequency.

In all panel response measurements it was necessary to restrict panel displacement to less than 0.005 in. (the panel thickness). If the displacement of a panel exceeds its thickness it may begin to behave as a membrane instead of a plate thus introducing non-linearities which lead to theoretical difficulty.

It was found that the measurements of panel response to acoustic excitation were not readily repeatable for supposedly identical panels and even repeated tests. This may be attributed to several factors: possible "oil-canning" of the panel; possible poor edge fixity; and temperature effects. Because of the relatively short period available for this whole project all these problems have not, as yet, been solved. Further work is required in this area to ensure repeatability of the results and resonance frequencies of the panel.

2.3.1.1 Simply-Supported Panel

For a simply-supported panel, the undamped resonance circular frequency for the m n mode is given by:

$$\omega_{mn} = \pi^2 h \left(\frac{m^2}{a^2} + \frac{n^2}{b^2}\right) \sqrt{\frac{E}{12 \rho (1 - \nu^2)}} \qquad (2)$$

where:

a	=	panel width
b	=	panel length
E	=	Young's modulus of elasticity
h	=	panel thickness
m	=	number of elastic half waves in x-direction
n	=	number of elastic half waves in y-direction
ρ	=	panel density
ν	=	Poisson's ratio

and taking the following values for the steel panel under investigation:

a	=	4 in.
b	=	8 in.
E	=	4.07×10^9 lb./ft.^{2}
h	=	0.005 in.
ρ	=	480 lb./ft.^{3}
ν	=	0.28

the panel fundamental resonance frequency is given by Equation (2):

$$f_{11} = \omega_{11}/2\pi = 36.1 \text{ Hz.}$$

2.3.1.2 Clamped-Clamped Panel

For a clamped-clamped panel, the undamped angular resonance frequency for the m n mode is given by:

$$\omega_{mn} = \frac{h}{b^2} \sqrt{R_{mn}} \sqrt{\frac{E}{12 \rho (1 - \nu^2)}} \qquad (3)$$

(see References 7 and 8)

where:

$$R_{mn} = \left(\frac{b}{a}\right)^4 \cdot \alpha_m^4 + \alpha_n^4 \quad 2 \left(\frac{b}{a}\right)^2 \cdot \psi_m \psi_n \qquad (4)$$

where α_m and ψ_m are resonance frequency parameters, for the m-th mode (see definitions in Reference 8), and taking the values above for the steel panel under investigation (and the following parameter values from Reference 8):

$$\alpha_1 = 4.73004$$

$$\psi_1 = 12.302$$

then the fundamental resonance frequency is given by Equation (3):

$$f_{11} = \omega_{11}/2\pi = 73.7 \text{ Hz.}$$

It is seen that in Figures 17 and 18, the fundamental resonance frequency seems to be about 60 Hz. Thus, although, the panel was designed to be clamped-clamped, from the above calculations it would appear that these edge conditions were not quite achieved in practice.

2.3.2 Panel Response to Attached Turbulent Boundary Layer Pressure Fluctuations

Figures 19 and 20 show the spectral density of the displacement of the center of the panel subjected to pressure fluctuations caused by an attached turbulent boundary layer (U_o = 144 fps). These measurements were made using the apparatus shown in Figures 15 and 16, respectively, with the exception that the microphone and thus oscillator and "compressor" parts of the circuits were eliminated.

These two measurements were made with different panels (of the same dimensions) and it is seen that the results are not repeatable. In particular, it is observed that one resonance which appears at approximately 125 Hz. in one measurement does not appear in the other. A two Hz. bandwidth filter was used for these measurements and a sweep time of greater than 30 minutes was employed. Due to non-repeatability of measurements further effort will have to be expended in determining the reasons and eliminating them in future experiments.

3.0 THEORETICAL PANEL RESPONSE

In this section of the report, the equations necessary to determine the response of panels to boundary layer pressure fluctuations are derived from first principles. These equations are given, in part, in Reference 3; however, for the sake of completeness they are also included herein, parts of the derivations being given more extended treatment to aid in clarity. In section 3.1, the equations giving panel response to random pressure fluctuations are derived, the method followed is in part similar to that of Reference 9, and the equations derived are identical to those obtained by Powell in Reference 10, [see Equations (4.3) and (5.4)]. However, in this section the equations are believed to be derived in a manner which is simpler to follow, although perhaps a little less rigorous. A more rigorous treatment may also be found in Appendix D of Reference 11. In section 3.1.1 the statistical properties of the boundary layer pressure field which must be determined in order to determine panel response are discussed and defined. Finally in section 3.1.2 the response of panels to boundary layer pressure fluctuations is discussed and the quantity, panel "joint-acceptance with the pressure field," is given. This joint acceptance has already been derived and is given in Reference 3; however, a much simpler derivation is given in full in Reference 11.

3.1 Response of Panels to Unsteady Pressure Fluctuations

When studying the response of panels to oscillatory loads it is customary to express the total response of the panel as a summation of the response of the individual modes of the panel. Provided the structural damping is small the modes can be assumed to respond independently to the pressure field and cross-coupling of modes can be neglected. Thus once the resonance frequencies and mode shapes have been determined, the problem is reduced to determining the responses of a set of single degree of freedom systems. The equation of motion defining the response of each mode is:

$$M_{mn}\ddot{q}_{mn}(t) + C_{mn}\dot{q}_{mn}(t) + K_{mn}q_{mn}(t) = F_{mn}(t) \qquad (5)$$

where: $q_{mn}(t)$ = generalized displacement coordinate of the mn mode

M_{mn} = generalized mass = $\rho h \int_x \int_y f^2_{mn}(x, y)\, dxdy$

C_{mn} = generalized damping coefficient = $2M_{mn}\omega_{o_{mn}}\delta_{mn}$

K_{mn} = generalized stiffness = $M_{mn}\omega^2_{o_{mn}}$

$F_{mn}(t)$ = generalized force at time t

$f_{mn}(x,y)$ = normalized mn mode shape of the panel

h = panel thickness

δ_{mn} = critical damping ratio for the mn mode = $\frac{1}{2Q_{mn}}$

ω_o = undamped resonance circular frequency of mn mode

and the subscripts:

m = number of elastic half waves in panel in x-direction

n = number of elastic half waves in panel in y-direction

The displacement of any point x, y on the panel at time t, may be expressed by the sum:

$$U(x,y,t) = \sum_{\substack{m=1 \\ n=1}}^{\infty} q_{mn}(t) \cdot f_{mn}(x,y) \tag{6}$$

For sinusoidal excitation of the form:

$$F_{mn}(t) = F_{o_{mn}} e^{i\omega t} \tag{7}$$

where: $F_{o_{mn}}$ is the amplitude of the generalized force (a real quantity), assume a solution of the form:

$$q_{mn}(t) = q_{o_{mn}} \cdot e^{i\left[\omega t - \beta(\omega/\omega_{o_{mn}})\right]} \tag{8}$$

where: $q_{o_{mn}}$ is the amplitude of the generalized displacement (a real quantity), and $\beta(\omega/\omega_{o_{mn}})$ is the phase angle between force and displacement.

On substituting Equations (7) and (8) into (5) and using the definitions for generalized quantities given above, the following is obtained:

$$q_{o_{mn}} = \frac{1}{M_{mn}\omega_{o_{mn}}^2} \cdot \frac{F_{o_{mn}} e^{i\beta\left(\omega/\omega_{o_{mn}}\right)}}{\left[1 - \left(\omega/\omega_{o_{mn}}\right)^2 + i\left(\omega/\omega_{o_{mn}}\right)/Q_{mn}\right]} \quad (9)$$

but for the amplitudes $q_{o_{mn}}$, $F_{o_{mn}}$ to be real quantities:

$e^{i\beta\left(\omega/\omega_{o_{mn}}\right)}\left[1 - \left(\omega/\omega_{o_{mn}}\right)^2 - i\left(\omega/\omega_{o_{mn}}\right)/Q_{mn}\right]$ must be a real quantity, and by expanding the exponential term into sine and cosine terms it may be shown that:

$$\tan\beta\left(\omega/\omega_{o_{mn}}\right) = \frac{\left(\omega/\omega_{o_{mn}}\right)/Q_{mn}}{1 - \left(\omega/\omega_{o_{mn}}\right)^2} \quad (10)$$

on substituting Equation (10) into (9):

$$q_{o_{mn}} = \frac{F_{o_{mn}}}{K_{mn}} \cdot H\left(\omega/\omega_{o_{mn}}\right) \quad (11)$$

where: $H\left(\omega/\omega_{o_{mn}}\right)$ is the single degree of freedom dynamic magnification factor

$$= \left\{\left[1 - \left(\omega/\omega_{o_{mn}}\right)^2\right]^2 + \left(\omega/\omega_{o_{mn}}\right)^2/Q_{mn}^2\right\}^{-\frac{1}{2}} \quad (12)$$

and thus from Equations (7), (8) and (11)

$$q_{mn}(t) = \frac{F_{mn}(t)}{K_{mn}} \cdot H\left(\omega/\omega_{o_{mn}}\right) e^{i\beta\left(\omega/\omega_{o_{mn}}\right)} \tag{13}$$

However, the actual displacement at a point x,y on a panel due to a force of frequency ω is given by:

$$W_{mn}(x,y,t;\omega) = f_{mn}(x,y) \cdot \frac{F_{mn}(t,\omega)}{K_{mn}} H\left(\omega/\omega_{o_{mn}}\right) e^{i\beta\left(\omega/\omega_{o_{mn}}\right)} \tag{14}$$

Now the generalized force is defined as:

$$F_{mn}(t;\omega) = \int_{x=0}^{a}\int_{y=0}^{b} P(x,y,t;\omega)\, f_{mn}(x,y,)\, dxdy \tag{15}$$

where: $P(x,y,t;\omega)$ = the sinusoidal pressure acting at the point x,y.

The mean-square value of the actual modal displacement is from (14):

$$\overline{W^2_{mn}(x,y,t;\omega)} = \frac{f^2_{mn}(x,y) \cdot F^2_{mn}(t;\omega)\; H^2\left(\omega/\omega_{o_{mn}}\right)}{K^2_{mn}} \tag{16}$$

where the mean-square value of the generalized force is:

$$\overline{F^2_{mn}(t;\omega)} = \int_{x=0}^{a}\int_{y=0}^{b}\int_{x'=0}^{a}\int_{y'=0}^{b} \overline{P(x,y,t;\omega) \cdot P(x',y',t;\omega)} \cdot f_{mn}(x,y) \cdot f_{mn}(x',y')dxdy \tag{17}$$

where x, y and x', y' are two independent points on the panel.

If the applied pressures contain several discrete frequency components, then the total mean-square displacement due to all frequency components is the summation of the mean-square displacement due to each frequency component. Furthermore, assume that the frequency content of the fluctuating pressures is limited to a very narrow band $\Delta\omega$, so that $\omega-\Delta\omega \leq \omega \leq \omega + \Delta\omega$, then the dynamic magnification factor $H\left(\omega/\omega_{o_{mn}}\right)$ may be assumed to be the same and a constant for all components in this narrow frequency band $\Delta\omega$. With this assumption, only the mean-square displacement $\overline{W^2_{mn}(x,y,t;\omega)}$ and the pressure cross correlation $\overline{P(x,y,t;\omega) \cdot P(x',y',t;\omega)}$ will vary with frequency in this band. Neglecting a rigorous mathematical proof, these two discrete frequency quantities are now replaced by their narrow band random equivalents which contain all frequency components in the $\Delta\omega$ band, their equivalents having the form:

$$\overline{W^2_{mn}(x,y,t;\omega,\Delta\omega)} \quad \text{and} \quad \overline{P(x,y,t;\omega,\Delta\omega) \cdot P(x',y',t;\omega,\Delta\omega)}$$

Assuming now that the magnitudes of these quantities are proportional to $\Delta\omega$, so that spectral densities may be assumed to exist then these narrow band quantities can be replaced by the displacement power spectral density $S_{w_{mn}}(x,y;\omega)$ and by the pressure cross power spectral density $S_p(x,y,x',y';\omega)$ respectively, (see for instance p. 12 of Reference 12). Thus, using Equation (17), Equation (16) can be written in the form to give the displacement power spectral density of the mn mode:

$$S_{w_{mn}}(x,y;\omega) = \frac{f^2_{mn}(x,y) \cdot H^2\left(\omega/\omega_{o_{mn}}\right)}{K^2_{mn}} \cdot$$

$$\cdot \int_{x=0}^{a} \int_{y=0}^{b} \int_{x'=0}^{a} \int_{y'=0}^{b} S_p(x,y,x',y';\omega)\, f_{mn}(x,y)\, f_{mn}(x',y')\,dx\,dy\,dx'\,dy' \tag{18}$$

Now it is convenient to express the pressure cross power spectral density as the product of a pressure spectrum level $S_p(\omega)$ and a normalized to unity cross-correlation function $R_p(x,y,x',y';\omega)$ where it must now also be assumed that the

pressure spectrum level is uniform over the panel surface. Making this substitution in Equation (18) and normalizing the range of integration gives:

$$S_{w_{mn}}(x,y;\omega) = \frac{f^2_{mn}(x,y)\, H^2\left(\omega/\omega_{o_{mn}}\right) \cdot S_p(\omega) \cdot J^2_{mn}(\omega) \cdot a^2\, b^2}{K^2_{mn}} \tag{19}$$

where: $J^2_{mn}(\omega)$ (the joint acceptance for the mn mode):

$$= \int_{\bar{x}=0}^{1} \int_{\bar{y}=0}^{1} \int_{\bar{x}'=0}^{1} \int_{\bar{y}'=0}^{1} R_p(\bar{x},\bar{y},\bar{x}',\bar{y}';\omega)\, f_{mn}(\bar{x},\bar{y}) \cdot f_{mn}(\bar{x}',\bar{y})\, d\bar{x}d\bar{y}d\bar{x}'d\bar{y}' \tag{20}$$

where: $\bar{x} = x/a$, $\bar{y} = y/b$, etc.

However, from previous definitions:

$$K_{mn} = M_{mn}\omega^2_{o_{mn}} = (\mu)ab\ \xi_{mn}\ \omega^2_{o_{mn}} \tag{21}$$

where: ξ_{mn} = generalized mass fraction for mn mode

μ = surface density of panel.

Thus from (21) and (19):

$$\frac{S_{w_{mn}}(x,y;\omega)}{S_p(\omega)} = \frac{f^2_{mn}(x,y) \cdot H^2\left(\omega/\omega_{o_{mn}}\right) \cdot J^2_{mn}(\omega)}{\mu^2\, \xi^2_{mn}\, \omega^4_{mn}} \tag{22}$$

and summing expressions of the form of Equation (22) for all the panel modes gives the total power spectral density of the panel displacement at a point (x,y):

$$\frac{S_w(x,y;\omega)}{S_p(\omega)} = \sum_{\substack{m=1 \\ n=1}}^{\infty} \frac{f^2_{mn}(x,y) \cdot H^2(\omega/\omega_{o_{mn}}) \cdot J^2_{mn}(\omega)}{\mu^2 \xi^2_{mn} \omega^4_{mn}} \qquad (23)$$

The power spectral density of the acceleration response $S_{\ddot{w}_{mn}}(x,y;\omega)$ can be obtained from the corresponding displacement by:

$$S_{\ddot{w}}(x,y;\omega) = \omega^4 S_w(x,y;\omega) \qquad (24)$$

3.1.1 Definition of Statistical Properties of the Turbulent Boundary Layer Forcing Field

Turbulent Boundary Layer Pressure Fluctuations

To calculate the response of a panel to turbulence it is seen from Equations (20) and (23) that it is first necessary to determine the following properties of the turbulent boundary layer pressure fluctuations:

i) The overall noise level
ii) The frequency spectrum
iii) The spatial correlation pattern and thus the convection velocity of the turbulent pressure field.

In the theoretical calculations made in this report, the ratio of the power spectral density of the response of the panel to the power spectral density of the pressure field is calculated (see Equation (23)). Thus in order to calculate this panel response ratio, it is first only necessary to determine the spatial correlation pattern and the convection velocity of the turbulent pressure field. Finally the actual panel response power spectral density may be obtained by multiplying by the power spectral density of the pressure field.

The Spatial Correlation Pattern and Convection Velocity

The spatial correlation pattern of the turbulent boundary layer describes the way in which the fluctuating pressures at different points in the pressure field are phased in relationship to each other. For structural response calculations, it has been shown by Wilby (Reference 3) that it is sufficient to determine the narrow

band space correlation functions in the longitudinal (flow) and lateral (normal to flow) directions separately. The product of these correlation functions then describes the spatial correlation field.

The narrow band longitudinal and lateral space correlation functions have been measured in wind tunnels at subsonic speeds by Bull (Reference 3) and other investigators (References 5, 13, 14, and 15). There is fair agreement between the measurements particularly the longitudinal correlations; the lateral correlations are not in such good agreement. Typical correlation curves are presented in Figures 21 and 22.

It is seen that the data in these curves have been collapsed on correlation Strouhal numbers of $\xi\omega/U_c$ and $\zeta\omega/U_c$ where ξ and ζ are the longitudinal and lateral separation distances, respectively, ω is the angular frequency, and U_c is the convection velocity of the pressure field.

It is possible to obtain good empirical fits for the experimental data and for the calculations in this report, these have been taken as:

$$R_p(\xi,0,0;\omega) = e^{-0.1\,(|\xi|\,\omega/U_c)} \cos(\xi\omega/U_c) \tag{25}$$

and

$$R_p(0,\zeta,0;\omega) = e^{-0.715\,(|\zeta|\,\omega/U_c)} \tag{26}$$

where R_p in Equations (25) and (26) are the longitudinal and lateral narrow band space correlation coefficients (with time delay zero).

Agreement between different measurements of $R_p(\xi,0,0;\omega)$ is good, and Figure 21 shows a typical result extracted from Reference 5. In Reference 15, Bakewell obtains the same result as Equation (25) with the coefficient of the exponential changed from -0.1 to -0.112. However, using a slightly different method Bull, in Reference 3, obtains an identical result to Equation (25) as follows:

The narrow band correlation coefficient is

$$R_p(\xi,\zeta,\tau;\omega) = \frac{Q_p(\xi,\zeta,\tau;\omega)}{Q_p(0,0,0;\omega)} \tag{27}$$

where $Q_p(\ )$ signifies the double pressure space-time covariance for a homogeneous wall pressure field. However, Equation (27) can be rewritten as:

$$R_p(\xi,\zeta,\tau;\omega) = \frac{\left|\phi_p(\xi,\zeta,\omega)\right| \cos(\omega\tau + \alpha)}{\phi_p(0,0,\omega)} \tag{28}$$

where $\phi_p(\ )$ is the cross spectral density of the pressure fluctuations and α is the phase angle of the cross spectral density.

It may also be shown that:

$$\alpha = -\frac{\omega\xi}{U_c}$$

which gives, on substituting into Equation (28), and for $\zeta = 0$ and $\tau = 0$:

$$R_p(\xi,0,0;\omega) = \frac{\left|\phi_p(\xi,0,\omega)\right| \cos(\omega\xi/U_c)}{\phi_p(0,0,\omega)} \tag{29}$$

but from Equation (28):

$$\left|R_p(\xi,0,\tau;\omega)\right| = \frac{\phi_p(\xi,0,\omega)}{\phi_p(0,0,\omega)} \tag{30}$$

Bull has made measurements of the amplitude of the correlation coefficient given by Equation (30) (see Figure 23). He also shows that a good assymptotic fit to the data at high frequency is given by:

$$\left| R_p(\xi,0,\tau;\omega) \right| = e^{-0.1\omega|\xi|/U_c} \qquad (31)$$

On substituting Equation (31) into (30) and then into Equation (29), it is observed that Equation (25) is again obtained.

In Figure 22 data from three separate experimental subsonic studies for lateral narrow band space correlations are given; a theoretical curve is also given. It is noticed that there is considerable scatter. However, two investigators find that

$$R_p(0,\zeta;\omega) = e^{-0.7\zeta\omega/U_c}$$

is a good fit to the data and the fit which Bull obtains (in Reference 3), namely Equation (26), is used in this Report.

It should be noticed that the narrow band data presented in Reference 5 have not been measured at values of $\omega\delta^*/U_c$ less than 0.2. There will be a lower cut-off frequency (ω), associated with an eddy diameter comparable with the boundary layer thickness, below which the empirical relations given in Equations (25) and (26) will become inaccurate. Thus, it is necessary to apply a weighting function to Equations (25) and (26) to prevent longitudinal and lateral correlation lengths and eddy diameters, associated with low frequencies, being predicted by Equations (25) and (26) to be much greater than the boundary layer thickness.

In Reference 3, Bull has measured the asymptotic values of the narrow band longitudinal and lateral correlation functions at which the narrow band longitudinal and lateral correlation Strouhal numbers $\omega\xi/U_c$ and $\omega\zeta/U_c$, respectively, approach zero, and these are shown in Figures 25 and 26. From these figures empirical fits were obtained and correction-factors applied which change Equations (25) and (26) into Equations (32) and (33) respectively:

$$R_p(\xi,0,0;\omega) = \left[e^{-0.1\left(|\xi|\omega/U_c\right)\cos\left(\xi\omega/U_c\right)} \right] e^{-0.265|\xi|/\delta} \qquad (32)$$

$$R_p(0,\zeta,0;\omega) = \left[e^{-0.715\left(|\zeta|\omega/U_c\right)} \right] e^{-2.0|\zeta|/\delta} \qquad (33)$$

where δ = boundary layer thickness.

It is seen both from Figures 23 and 24 and the empirical fits to these curves [given by Equations (33) and (34)] that for eddies associated with low frequencies, the lateral and longitudinal correlation functions are independent of frequency, while for eddies associated with high frequencies the correlation functions are frequency dependent. The demarcation between frequency independence and frequency dependence may easily be determined from Equations (33) and (34).

Longitudinal Correlation Demarcation Frequency:

This may easily be determined from Equation (33) by putting:

$$0.1\,|\xi|\,\omega/U_c = 0.265\,|\xi|/\delta$$

$$\omega = 2.65\,U_c/\delta$$

or eddy wavelength (in stream direction):

$$\lambda = \frac{2\pi}{2.65}\,\delta = 2.37\,\delta$$

$$\lambda \approx 2\,\delta$$

Lateral Correlation Demarcation Frequency:

Similarly this is determined from Equation (33) by putting:

$$0.715\,|\zeta|\,\omega/U_c = 2.0\,|\zeta|/\delta$$

$$\omega = 2.80\,U_c/\delta$$

or eddy wavelength (in stream direction):

$$\lambda = \frac{2\pi}{2.8}\,U_c/\delta = 2.24\,\delta$$

$$\lambda \approx 2\,\delta$$

Bull obtains the same result in Reference 3 , although by a slightly different argument. From this result and some other experimental measurements Bull suggests (in Reference 3) that the turbulent boundary layer pressure field consists of two families of pressure eddies. One family comprises small scale fluctuation components convected near to the wall which lose coherence in the time taken for them to be convected about 4 wavelengths. Their longitudinal and lateral narrow band correlations are functions of $\omega\xi/U_c$ and $\omega\zeta/U_c$ respectively. The other family comprises large scale fluctuations (associated with motion at distances greater than 0.1 to 0.15 δ from the wall) which lose coherence as a group. The rate of loss of coherence is independent of wavelength and these eddies persist for much longer times than the small scale fluctuations .

The demarcation between large and small pressure eddies occurs at a longitudinal convection wavelength of about 2δ; the fact that both narrow band longitudinal and lateral correlation measurements (Figures 23 and 24) and empirical fits [Equations (32) and (33)] give this result adds confidence in the consistency of these results.

For calculations of panel response at supersonic speeds, narrow band space correlation data for supersonic turbulent boundary layers are not readily available at the present time; however, some broad band longitudinal and lateral space correlation functions have been measured (Reference 17). It is observed (Figure 27) that the longitudinal space correlation functions at Mach numbers of 0.59 and 3.45 (when the data from Reference 17 are corrected for momentum thickness and convection velocities–see Figure 28) collapse well on the parameter ξ/U_c . This suggests that Equations (25) and (26) are probably good empirical expressions for the correlation functions at supersonic as well as subsonic speeds.

The turbulent boundary layer may be regarded (Figure 29) as a gradually decaying pressure field convected downstream with a velocity (U_c) somewhat less than that of free-stream (U_o) . The convection velocity is higher for large eddies (associated with low frequencies (ω) and is about $0.9\ U_o$ for subsonic flow; for small eddies (associated with high frequencies ω) the convection velocity is lower and is asymptotic to $U_c = 0.6\ U_o$, for subsonic flow. This is because the large eddies are situated near the edge of the boundary layer and the small eddies near to the wall (Figure 30). The mean (or wide-band) convection velocity is about 0.8 for subsonic flow. Figure 28 extracted from Reference 6, shows the variation of mean convection velocity with Mach number and this mean velocity is used in the structural calculations. It should be noted that more recent results (Reference 17) demonstrate an increase in U_c from $0.6\ U_o$ at subsonic speeds to $0.95\ U_o$ at supersonic speeds. Also, convection velocity has been shown (Reference 3) to depend also upon frequency

and spatial separation of the measuring transducers. There is therefore, some doubt as to the correct value of U_c to use. Further experimental study is required of this phenomenon and awaiting this, the results of Figure 28 have been utilized.

3.1.2 Response of Panels to Turbulent Boundary Layer Pressure Fluctuations

For a turbulent boundary layer the cross correlation function $R_p(x,y,x',y';\omega)$ which may be written as a product of Equations (32) and (33) may be written in the form:

$$R_p(x,y,x',y';\omega) = e^{-\delta_x |\bar{\xi}|} \cdot \cos(\gamma_x \bar{\xi}) \cdot e^{-\delta_y |\bar{\zeta}|} \cos(\gamma_y \bar{\zeta}) \tag{34}$$

where:

$$\left.\begin{array}{ll|ll} \delta_x = 0.10\omega a/U_c + 0.265\, a/\delta & & \delta_y = 2\omega b/U_c + 2b/\delta & \\ \gamma_x = \omega a/U_c & & \gamma_y = 0 & \\ \bar{\xi} = \xi/a = \bar{x} - \bar{x}' & & \bar{\zeta} = \zeta = \bar{y} - \bar{y}' & \\ \bar{x} = x/a & & \bar{y} = y/b & \end{array}\right\} \tag{35}$$

For a cross correlation function of the form of Equation (34) Wilby shows in Reference 3 that Equation (20) integrates to give (for a simply-supported panel):

$$J^2_{mn}(\omega) = 4\Phi_x \Phi_y/(mn\pi^2)^2 \tag{36}$$

where:

$$\Phi_x = \frac{1}{\Delta_x^2}\left\{p_x\left[1-(-1)^m e^{-\delta_x}\cos\gamma_x\right] + 4(-1)^m q_x e^{-\delta_x}\sin\gamma_x + \frac{m\pi}{2} r_x \Delta_x\right\}$$

$$\left.\begin{aligned}
\Delta_x &= \left[1+\left(\frac{\delta_x}{m\pi}\right)^2 + \left(\frac{\gamma_x}{m\pi}\right)^2\right]^2 - 4\left(\frac{\gamma_x}{m\pi}\right)^2 \\
p_x &= \left[1+\left(\frac{\delta_x}{m\pi}\right)^2 - \left(\frac{\gamma_x}{m\pi}\right)^2\right]^2 - 4\left(\frac{\gamma_x}{m\pi}\right)^2\left(\frac{\delta_x}{m\pi}\right)^2 \\
q_x &= \left(\frac{\delta_x}{m\pi}\right)\left(\frac{\gamma_x}{m\pi}\right)\left[1+\left(\frac{\delta_x}{m\pi}\right)^2 - \left(\frac{\gamma_x}{m\pi}\right)^2\right] \\
r_x &= \left(\frac{\delta_x}{m\pi}\right)\left[1+\left(\frac{\delta_x}{m\pi}\right)^2 + \left(\frac{\gamma_x}{m\pi}\right)^2\right]
\end{aligned}\right\} \quad (37)$$

and Φ_y, Δ_y, p_y, q_y, and r_y are given by Equations (37) above where x is replaced by y and m by n.

The method used by Wilby involves a rather long tedious algebraic manipulation and Crocker and White derive the same results, by a much simpler method in Reference 11. However, the results are presented in Equations (36) and (37) in the form given by Wilby for convenience of digital computer evaluation. The computer program which was used to compute Equations (23) and (24), making use of Equations (35), (36) and (37), is given in Appendix A.

Evaluations of Equations (23) and (24), by the computer program discussed in Appendix A, were made for the panel and flow conditions used in the experiment (although the panel had to be assumed simply supported). The theoretical computations and comparisons between theoretical predictions and experimental measurements are discussed in Section 4.0 of this report.

4.0 DISCUSSION

4.1 Theoretical Computations of Panel Response

Using the theory developed in Section 3.0 of this report (Equations (23), (24), and (35) through (37)) and the computer program (Appendix A) designed to evaluate this theory, calculations were made which should be representative of the response of the panel to the turbulent boundary layer flow of the experimental setup. However, it should be noted that in the experiment, the panel was designed to have fully-fixed edges, while the theory assumes simply-supported edges.

The inputs which were assumed for the experiment, and hence the computer program, were:

$a = 4$ in. $= 1/3$ ft.

$b = 8$ in. $= 2/3$ ft.

$E = 4.07 \times 10^9$ lb/ft.^{2}

$h = 0.005$ in. $= 0.000417$ ft.

$I = \frac{1}{12} (1) (0.005)^3 = 10.42 \times 10^{-9}$ in.^{3}

$U_c = 144 \times 0.8 = 115.2$ fps $= 1382.4$ ips

$Q = \frac{1}{2\delta} = 50$

$\rho = 480$ lb./ft.$^3 = 0.278$ lb./in.^{3}

$\mu = 0.200$ lb./ft.$^2 = 0.00139$ lb./in.$^2 = \rho h$

$\nu = 0.28$

$x/a = 0.5$

$y/b = 0.5$

$\delta = 12$ in.

Using these inputs Equation (2) may be written (after some rearrangement) to give the resonance frequencies for the panel used in the experiment (assuming simple-supported edges); thus,

$$f_{mn} = \frac{\pi}{2} \left(\frac{m}{a}\right)^2 \left[1 + \left(\frac{n}{m}\right)^2 \left(\frac{a}{b}\right)^2\right] \sqrt{\frac{g E I}{\mu (1 - \nu^2)}} \qquad (38)$$

$$f_{mn} = 29.2\ m^2 \left[1 + \frac{1}{4}\left(\frac{n}{m}\right)^2\right] \qquad (39)$$

Thus:

$$f_{11} = 36.5 \text{ Hz.}; \quad f_{6,1} = 1025 \text{ Hz.}; \quad f_{19,1} = 10{,}540 \text{ Hz.}$$

$$f_{1,12} = 1040 \text{ Hz.}; \quad f_{1,38} = 10{,}170 \text{ Hz.}$$

The computer program was run twice, once to calculate panel displacement and acceleration up to 1,000 Hz. and second to calculate response up to 10,000 Hz. The second run was mainly to study the effects of longitudinal coincidence which was expected to occur at about 1,000 Hz. (see discussion below). Since the center of the panel was chosen ($x/a = y/b = 0.5$) only odd modes were included in the computer calculation. From the frequencies calculated above, for the first computer run, m was allowed to assume values of 1, 3, and 5, and n, values of 1, 3, 5, 7, 9, and 11, a total of 18 modes only. In this first computer run, since the number of modes summed was small the frequency increments were kept small in order to increase the accuracy of calculations (0.25 Hz. up to 250 Hz, and 1 Hz. from 250 to 1,000 Hz.). In the second computer run, m was allowed to assume values of 1, 3, 5, ... 17, 19, and n, values of 1, 3, 5, ... 35, 37, a total of 171 modes being summed for each response point against frequency calculated. In order to reduce computation time the frequency increments were increased, particularly at high frequencies, (1 Hz. up to 250 Hz., 2 Hz. from 250 Hz. to 1,000 Hz. and 10 Hz. from 1,000 Hz. to 10,000 Hz.). It was found, however, that the two computer runs gave identical plots (over the same frequency ranges covered) except for the first made which was predicted more accurately by the first computer run. Thus the two computer runs have been combined into the two figures showing displacement and acceleration response (in Figures 31 and 32 respectively).

It is noticed that the programs were run with a value of boundary layer thickness $\delta = 12$ in. This was an error, as it was intended to run the program with a more representative value of $\delta = 1$, or 2 in. This error probably results in a small increase in the estimated response of the first few panel modes and will be eliminated in future runs.

The panel response at the first resonance was checked by a hand calculation and agreed closely with the response calculated by the computer program.

Longitudinal Coincidence

The most striking aspect of panel response to turbulent boundary layer pressure fluctuations is longitudinal coincidence. This occurs when the longitudinal

bending wave propagation velocity in the panel equals the velocity of convection of the pressure disturbances.

Using the notation and panel dimensions used above and in Appendix C, the resonance frequencies of the panel (assumed simply-supported) are (see above):

$$f_{mn} = \frac{\pi}{2}\sqrt{\frac{EI}{\mu(1-\nu^2)}}\left(\frac{m}{a}\right)^2\left[1+\left(\frac{n}{m}\right)^2\left(\frac{a}{b}\right)^2\right] \tag{38}$$

$$f_{mn} = 29.2\ m^2\left[1+\frac{1}{4}\left(\frac{n}{m}\right)^2\right] \tag{39}$$

But for coincidence, the convection velocity (see Reference 9):

$$U_c = C_m = \lambda_m f_m \tag{40}$$

$$U_c = (2a/m)\ f_m \tag{41}$$

where

λ_m = bending wave length of the m-th longitudinal mode of the panel.

f_m = resonance frequency of the m-th longitudinal mode of the panel

= $29.2\ m^2$.

With a convection velocity of $144 \times 0.8 = 115.2$ fps

$$U_c = (2a/m)\ f_m \tag{41}$$

$$115.2 \times 12 = (2 \times 4/m)\ (29.2\ m^2),\quad m \approx 6$$

$$f_{coinc.} \approx 29.2\ (6)^2 \quad 1050\ \text{Hz}.$$

The two computer plots of panel response shown in Figures 31 and 32 do indeed show that the acceleration and displacement power spectral density drop off considerably after this frequency.

One feature of the panel response not included in the present theory was the effect of non-linearities due to membrane stiffness. This effect becomes significant when the displacement of the panel exceeds the panel thickness. Typically the panel displacement was about 6 times the thickness for the first mode response. Approximate

calculations suggest that the displacement of the first mode will be reduced by a factor of about 2 over that predicted. Higher order modes are relatively unaffected.

4.2 Comparison of Experimental Results with Theoretical Predictions

Figures 19 and 20 present the raw experimental data on panel displacement spectrum without normalization by the acoustic pressure spectrum given in Figures 9 and 10. When the data are normalized and compared to the theoretical results given in Figure 31, the latter are found to be appreciably higher. A number of reasons exist for this discrepancy which may be summarized as follows:

- The panel response was very likely nonlinear due to the very small thickness-to-span ratio.
- Buckling or "oil canning" of the panel is expected to contribute to a reduced response.
- The experimental data in Figures 19 and 20 indicate that the panel resonance corresponded more nearly to a simply supported panel than a clamped panel as intended. Although this is the same boundary condition used for the theoretical plots, the effect of radiation damping, calculated in Appendix C for the simply supported panel, indicates that the panel Q should be no more than about 8 instead of 50 as assumed for the theory.
- The validity of the acoustic spectrum is in question as discussed in Section 2.3 so that the effective acoustic pressure spectrum on the panel is in doubt.
- It is also seen (in Figures 9 and 10) that the pressure frequency spectrum achieved in the experiment was not typical of a normal turbulent boundary layer, and it is probable that the pressure spatial correlation patterns set up in the experiment were dissimilar to those assumed in the theoretical analysis. This fact will obviously affect panel response and attention will have to be given to investigating the boundary layer pressure fluctuation spectrum and pressure correlation pattern, in more detail, in future work.

Clearly, there are several important disagreements between the theory and the experiment. Unfortunately, there has not been sufficient time available to eliminate all the problems associated with the experimental measurements. A more detailed study is recommended based on a knowledge of the difficulties found in the work to date.

5.0 CONCLUSIONS

A powerful theoretical method has been developed which predicts simply-supported panel response to turbulent boundary layer pressure fluctuations. The analysis has been programmed for computation by a digital computer and computer plots of panel response and a listing of the program are presented in this report. Considerable progress has been made in understanding the statistical properties of the turbulent boundary pressure fluctuations which must be determined for theoretically predicting panel response to turbulence (Section 3). For full scale structures, it is now realized that it is necessary to apply a weighting function to the empirical expressions for the narrow band pressure space correlations, in order to prevent correlation lengths much greater than the boundary layer thickness being predicted (a physically unlikely situation).

Considerable success has been achieved in setting up suitable repeatable separated flow which will be required for later panel response measurements and the basic flow patterns have been externally examined. However, some difficulties have been experienced in panel response measurements. These difficulties are associated with the non-uniformities of the panel tested, and the results are not typical of uniform panels. However, the experimental techniques required have been developed successfully during the present work. Repetition of the experiments with a more uniform panel can be expected to give useful data. The theoretical analysis is now highly developed, and confirmation of the theoretical results by an experiment will be of much value.

6.0 ACKNOWLEDGEMENTS

The author would like to thank Mr. D. Hardrove and Mr. P. Rhodes of the Wyle Computation Staff who developed the computer program, the listing of which is given in Appendix A, and also Mr. J. Wilson and Mr. N. Esslinger for their assistance in measurements of panel response.

The author is also grateful to Mr. R. White and Dr. M. Lowson for a critical examination of the draft report.

REFERENCES

1. G. Young and T. Shiokari, "Buffeting Data Obtained on Mercury/Atlas MA-2 and MA-3", Report Number TDR 594 (1101) TN-1, August 1961.

2. M. J. Crocker, "Response of Panels to Oscillating Shock Waves", Wyle Laboratories Research Staff Report WR 66-17, (NASA N66-35170), March 1966.

3. M. K. Bull, J. F. Wilby, and D. R. Blackman, "Wall Pressure Fluctuations in Boundary Layer Flow and Response of Simple Structures to Random Pressure Fields", University of Southampton AASU Report Number 243, July 1963.

4. M. Y. ElBaroudi, G. R. Ludwig, and H. S. Ribner, "An Experimental Investigation of Turbulence - Excited Panel Vibration and Noise (Boundary-Layer Noise)", NATO Advisory Group for Aero Research and Development, Report 465, April 1963.

5. L. Maestrello, "Measurement and Analysis of the Response Field of Turbulent Boundary Layer Excited Panels", J. Sound Vibration (1965) 2 (3), pp 270-292.

6. A. L. Kistler and W. S. Chen, "A Fluctuating Pressure Field in a Supersonic Turbulent Boundary Layer", J. Fluid Mech., Vol. 16, Part 1, May 1963.

7. R. W. White, "Vibration Characteristics of Beams and Plates Mounted on Elastic and Inertial Supports", Wyle Laboratories Research Staff Report WR 64-2, August 1964.

8. M. J. Crocker, "Theoretical and Experimental Response of Panels to Traveling Sonic Boom and Blast Waves", Wyle Laboratories Research Staff Report WR 66-2, March 1966.

9. R. W. White and M. J. Crocker, "Preliminary Analysis of the Effects of Pressure Space Correlations on the Vibrations of Apollo Flight Structure", Wyle Laboratories Research Staff Report WR 66-32, May 1966.

10. A. Powell, "On the Response of Structures to Random Pressures and to Jet Noise in Particular", Chapter 8 of "Random Vibration", Volume 1, Edited by S. H. Crandall, the M.I.T. Press., January 1964.

11. M. J. Crocker and R. W. White, "Response of Lockheed L-2000 Supersonic Transport Fuselage to Turbulence and to Reverberant Noise", Wyle Laboratories Research Staff Consulting Report Number WRC 66-11, September 1966.

12. S. H. Crandall, "Mechanical Vibrations with Deterministic Excitation", Chapter 1 of "Random Vibration", Volume 1, Edited by S. H. Crandall, the M.I.T. Press, January 1964.

13. T. H. Hodgson, "Pressure Fluctuations in Shear Flow Turbulence", Ph.D. Thesis, University of London, May 1962.

14. H. P. Bakewell, "Narrow Band Investigations of the Longitudinal Space-Time Correlation Function in Turbulent Airflow", J. Acoust. Soc. Am. 36, 146-148, 1964.

15. W. W. Willmarth and C. E. Wooldridge", Measurements of the Fluctuating Pressure at the Wall Beneath a Thick Turbulent Boundary Layer", J. Fluid. Mech., Vol. 14, Part 2, October 1962.

16. S. Gardner, "On Surface Pressure Fluctuations Produced by Boundary Layer Turbulence", Acustica Vol. 16, Number 2, 1965/1966.

17. W. V. Speaker and C. M. Ailman, "Spectra and Space-Time Correlations of the Fluctuating Pressures at a Wall Beneath a Supersonic Turbulent Boundary Layer Perturbed by Steps and Shock Waves", Report SM-49806, November 1965.

18. D. Bozich, " Radiation Damping of Panels Mounted in Ducts", Wyle Laboratories Research Staff Report WR 64-4, 1965.

APPENDIX A

LOGIC FOR THE DIGITAL COMPUTER PROGRAM TO CALCULATE STRUCTURAL RESPONSE TO TURBULENT BOUNDARY LAYER PRESSURE FLUCTUATIONS

A computer program was written to calculate the ratio of displacement power spectral density to pressure spectral density, and acceleration power spectral density to pressure spectral density, for any point on the panel, as given by Equations (23) and (24), respectively. The subroutine JMN (Omega) given on the last page of the computer listing calculates the joint-acceptance as given by Equations (35) through (37). A Flow Chart of the computer program is given in Figure A 1. A listing of the computer program is given in Figure A 2.

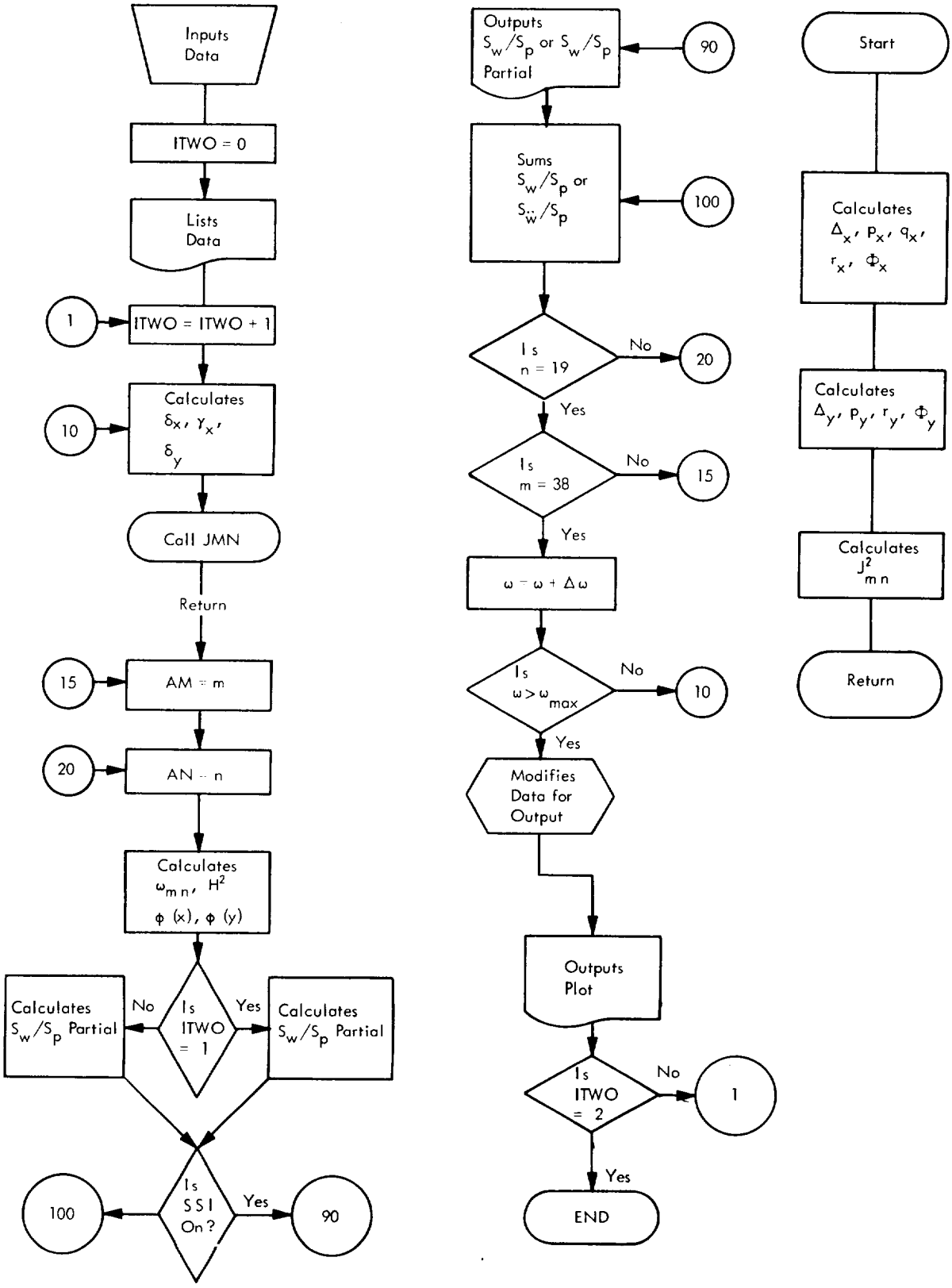

Figure A1. Flow Chart for Computer Program

```
                                        3200  FORTRAN     (2.1)

      PROGRAM TURB
C
C     PANEL RESPONSE TO TURBULENT BOUNDARY LAYER PRESSURE FLUCTUATIONS.
C     ANALYSIS BY MALCOLM CROCKER.......PROGRAMMING BY DAVE HARGROVE.
C
      COMMON AJ(20,40),AX,AY,BX,BY,PD,H,PLX,PLY,X,Y
     1,M,N,E,PI,G,Q
      COMMON    SW(1600),OMA(1600)
      PI=3.14159265
      AK3=.3575 $ PITWO=PI*PI  $ PI200=PI*440.
      CALL OVERFL(I)
      ITWO = 0
      G=386.0
      E=2.82E 07
      READ (60,1010) RNUM,DEL
      DEL=12.
      READ(60,1001) M,N
      WRITE (61,1010) RNUM,DEL
      WRITE (59,1010) RNUM,DEL
      WRITE (61,1001) M,N
      WRITE (59,1001) M,N
    1 CALL READCON
      READ(60,1000) UC,TMU,TI,X,Y,DOMA,OMAMAX,PLX,PLY,Q
      ITWO = ITWO+1
                              CUT3=OMAMAX*20000.*PI $ M=19 $ N=37
      DEL1=2.*PI
      DEL2=4.*PI
      DEL3=20.*PI
      CUT1=500.*PI
      CUT2=2000.*PI
      WRITE(61,1000)UC,TMU,TI,X,Y,DOMA,OMAMAX,PLX,PLY,Q
      AK1=AK2=1.0
      AK4=0.
      OMA(1)=1.0
      K=0
      PIX=PI*X  $  PIY=PI*Y  $PI2=PI*PI  $Q2=Q*Q  $G2=G*G
      XII=YII=1.042E-08
      TMU2=TMU*TMU
      SQRXII=SQRTF(XII) $  SQRYII=SQRTF(YII)
      RY=0.
   10 K=K+1
      AX=.1*OMA(K)/UC+.265/DEL
      BX=AK2*OMA(K)/UC
      AY=2.*AK3*OMA(K)/UC +2./DEL
      OMEGA = OMA(K)
      CALL JMN(OMEGA)
      SW(K)=0.0
      XM=-1.
      DO 100 I=1,M,2
      XM=XM+2.
      XN=-1.
      DO 100 J=1,N,2
      XN=XN+2.
      W=PI2* SQRTF(G*E/TMU)
      TEMP=((XM*XM)/(PLX*PLX))*SQRXII *XN*XN*SQRYII/(PLY*PLY)
      W=W*TEMP
      W2=W*W  $  W4=W2*W2
      PSI=SIN(XM*PIX/PLX)*SIN(XN*PIY/PLY)
      PSI2=PSI*PSI  $ TEMP=OMA(K)/W
      H2=1./((1.-(OMA(K)/W)**2)**2 + TEMP*TEMP/Q2)
```

Figure A2 Listing of Computer Program

```
      GO TO (87,88) ITWO
   87 TEMP=G2*PSI2*AJ(I,J)*H2/(TMU2*.0625*W4)
      GO TO 91
   88 TEMP=PSI2*AJ(I,J)*H2 / (TMU2 * W4 * .0625)
      TEMP=TEMP * OMA(K) **4
   91 GO TO (90,100) ,SSWTCHF(1)
   90 WRITE (61,1002) TEMP,I,J,OMA(K)
  100 SW(K)=SW(K)+TEMP
      IF (OMA(K).LE.CUT1) 110,120
  110 OMA(K+1)=OMA(K)+DEL1 $ GO TO 10
  120 IF (OMA(K).LE.CUT2) 130,140
  130 OMA(K+1)=OMA(K) + DEL2 $ GO TO 10
  140 IF (OMA(K).LE.CUT3) 142,146
  142 OMA(K+1)=OMA(K) + DEL3 $ GO TO 10
  146 CONTINUE
      CALL PRINTCON
      WRITE (61,1005) (SW(I),I=1,K)
      WRITE(61,1003) SW(K),OMA(K)
      WRITE (61,1005) (OMA(I),I=1,K)
      DO 150 I=1,K
      OMA(I)=ALOG(OMA(I)*5.00/PI)*2.0*.43429448
  150 SW(I)=ALOG(SW(I)*1.0E-02)*.43429448
      WRITE(61,1003) SW(K),OMA(K)
      CALL PLOTCON
      CALL LOGAXIS(0.0,6.0,1.0,1.0,0)
      CALL PLOT(0.0,6.0,-3)
      CALL LOGAXIS(0.0,6.0,1.0,1.0,0)
      CALL LOGAXIS(8.0,0.0,2.0,2.0,0)
      DO 170 J=1,K
      IF (OMA(J).LT.BNUM) 170,160
  170 CONTINUE
  160 X=OMA(J)-BNUM
      CALL PLOT (X,SW(J),3)
      DO 165 KK=J,K
      X=OMA(KK)-BNUM
  165 CALL PLOT (X,SW(KK),2)
      CALL PLOT(0.0,8.0,-3)
      CALL PRINTCON
      IF (ITWO.GE.2)  300,1
  300 CONTINUE
      WRITE(59,1004)
      STOP
 1000 FORMAT(5E16.8)
 1001 FORMAT(5I3)
 1002 FORMAT(5X21HTHE VALUE OF WD/WP ISE16.8,8H, FOR M=I2,7H AND N=I2,
     15X,11H AND OMEGA=,1X,E16.8)
 1003 FORMAT(5X,6HSW/SP=E16.8,5X6HOMEGA=E16.8/)
 1004 FORMAT(5X,7HTHE END/)
 1005 FORMAT (10X,7E16.8,/)
 1010 FORMAT (2F10.0)
      END

        3200 FORTRAN DIAGNOSTIC RESULTS - FOR   TURB


NO ERRORS
```

Figure A2 (Continued)

```
      SUBROUTINE JMN(OMEGA)
      COMMON AJ(20,40),AX,AY,BX,BY,PD,H,PLX,PLY,X,Y
     1,M,N,E,PI,G,Q
      DIMENSION XX(20),YY(40)
      DIMENSION OMA(1)
      K=1  $ OMA(K)=OMEGA
      AXLX=AX*PLX
      BXLX=BX*PLX
      XM=-1.$ AXLX2=AXLX*AXLX  $  BLX2= BXLX*BXLX
      DO 10 I=1,M,2
      XM=XM+2.
      BOT=XM*PI  $ BOT2=BOT*BOT
      A2=AXLX2/BOT2
      B2=BLX2/BOT2
      TEMP=1.+A2+B2
      TEMP2=TEMP*TEMP
      DX=TEMP2-4.*B2
      TEMP1=1.+A2-B2
      TEMP3=TEMP1*TEMP1
      PX=TEMP3-4.*A2*B2
      GX=AXLX*BXLX*TEMP1/BOT2
      VX=AXLX*TEMP/BOT
      GO TO (5,10) ,SSWTCHF(1)
    5 WRITE(61,1001) DX,PX,GX,VX,I
      WRITE (61,1003) OMEGA
   10 XX(I)=1.0/(DX**2)*(PX*(1.0-(-1.0)**I*EXP(-AXLX)*COS(BXLX))
     1+4.0*GX*(-1.0)**I*EXP(-AXLX)*SIN(BXLX)*BOT/2.0*VX*DX)
      AYLY=AY*PLY
      BYLY=BY*PLY
      XN=-1.
      DO 20 I=1,N,2
      XN=XN+2.
      J=I
      BOT=XN*PI
      A2=(AYLY/BOT)**2
      B2=(BYLY/BOT)**2
      DY=(1.0+A2+B2)**2-4.0*B2
      PY=(1.0+A2-B2)**2-4.0*A2*B2
      GY=(AYLY/BOT)*(BYLY/BOT)*(1.0+A2-B2)
      VY=AYLY/BOT*(1.0+A2+B2)
      GO TO (15,20) ,SSWTCHF(1)
   15 WRITE(61,1000) DY,PY,GY,VY,I
      WRITE (61,1003) OMEGA
   20 YY(I)=1.0/(DY**2)*(PY*(1.0-(-1.0)**J*EXP(-AYLY)*COS(BYLY))
     1+4.0*GY*(-1.0)**J*EXP(-AYLY)*SIN(BYLY)*BOT/2.0*VY*DY)
      AM=-1.
      DO 30 I=1,M,2
      AM=AM+2.
      AN=-1.
      DO 30 J=1,N,2
      AN=AN+2.
      AJ(I,J)= 4.0*XX(I)*YY(J)/((AM*AN*PI**2)**2)
      GO TO (25,30) ,SSWTCHF(1)
   25 WRITE(61,1002) AJ(I,J),I,J
   30 CONTINUE
      RETURN
 1000 FORMAT(5X11HDY,PY,GY,VY/(4E16.8,I3))
 1001 FORMAT(5X11HDX,PX,GX,VX/(4E16.8,I3))
 1002 FORMAT(5X,12HJMN(OMA),I,J/(E16.8,2I3))
 1003 FORMAT (5X,6HOMEGA=,1X,E16.8)
      END
```

Figure A2 (Concluded)

APPENDIX B

BIBLIOGRAPHY ON PANEL RESPONSE TO TURBULENT BOUNDARY LAYER PRESSURE FLUCTUATIONS

1. H.S. Ribner; "The Noise of Aircraft," UTIAS Review No. 24 AFOSR 64-1310, August 1964.

2. M.Y. el Bardoudi, G.R. Ludwig and H.S. Ribner; "An Experimental Investigation of Turbulence - Excited Panel Vibration and Noise (Boundary-Layer Noise)," NATO Advisory Group for Aero Research and Development, Report 465, April 1963.

3. M.K. Bull, J.F. Wilby and D.R. Blackman; "Wall Pressure Fluctuations in Boundary Layer Flow and Response of Simple Structures to Random Pressure Fields," University of Southampton, AASU Report No. 243, July 1963.

4. G.R. Ludwig; "An Experimental Investigation of the Sound Generated by Thin Steel Panels Excited by Turbulent Flow (Boundary Layer Noise)," Institute of Aerophysics, University of Toronto, UTIA Report No. 87, November 1962.

5. G.T. Kantarges; "Some Measurements of Noise Transmission and Stress Response of a 0.020-Inch Duraluminum Panel in the Presence of Air Flow," NASA TN D-459, September 1960.

6. H.S. Ribner; "Boundary-Layer-Induced Noise in the Interior of Aircraft," UTIA Report No. 37, Institute of Aerophysics, University of Toronto, April 1956.

7. G.B. Warburton; "Vibration of Rectangular Plates," Proc. Inst. Mech. Engrs. (London), Vol. 168, No. 12, 1953, pp. 371-384.

8. D.H. Tack and R.F. Lambert; "Response of Bars and Plates to Boundary Layer Turbulence," Journal of the Aerospace Sciences, Vol. 29, No. 3, March 1962.

9. I. Dyer; "Response of Plates to a Decaying and Convecting Random Pressure Field," J. Acoust. Soc. Am., Vol. 31, No. 7, July 1959.

10. M. Strasberg; "Response of Plates and Membranes to Pressure Fluctuations of a Turbulent Boundary Layer," J. Acoust. Soc. Am., Vol. 30, No. 7, July 1958, p. 680 (Abstract).

11. A. Powell; "On the Fatigue Failure of Structures Due to Vibrations Excited by Random Pressure Field," J. Acoust. Soc. Am., Vol. 30, No. 12, December 1958.

12. G.M. Corcos and H.W. Liepmann; "On the Contribution of Turbulent Boundary Layers to the Noise Inside a Fuselage," NACA TM 1420, December 1956.

13. R.A. Mangiarotty; "Acoustic Radiation Damping of Vibrating Structures," J. Acoust. Soc. Am., Vol. 35, No. 3, March 1963.

14. L. Maestrello; "Measurement and Analysis of the Response Field of Turbulent Boundary Layer Excited Panels," J. Sound. Vib., (1965)2 (3), pp. 270-292.

15. L. Maestrello; "Measurement of Noise Radiated by Boundary Layer Excited Panels," J. Sound Vib. (1965) 2 (2), pp. 100-115.

16. J.F. Wilby; "Turbulent Boundary Layer Pressure Fluctuations and Their Effect on Adjacent Structures," Sonderdruck aus dem Jahrbuch 1964 der WGLR.

17. E.J. Richards and J.F. Wilby; "Proceedings of Second International Conference on Acoustical Fatigue in Aerospace Structures," Dayton, Ohio, 1964.

18. D.A. Bies; "A Wind Tunnel Investigation of Panel Response to Boundary Layer Pressure Fluctuations at Mach 1.4 and Mach 3.5," B.B. & N. Report No. 1264, Douglas Prime Subcontract DAC-A-64-432, NASA Prime Contract NASW-932.

19. D.J. Bozich; "Spatial Correlation in Acoustic Structural Coupling," J. Acoust. Soc. Am., Vol. 36, No. 1, January 1964.

20. H.S. Ribner; "Response of a Flexible Panel to Turbulent Flow: Running Wave versus Modal-Density Analysis," J. Acoust. Soc. Am., Vol. 40, No. 3, September 1966.

21. P.H. White and A. Powell; "Transmission of a Random Sound and Vibration Through a Rectangular Double Wall," J. Acoust. Soc. Am., Vol. 40, No. 4, October 1966.

22. M.Y. el Baroudi; "Turbulence-Induced Panel Vibration," University of Toronto, UTIAS Report No. 98, February 1964.

23. J.E. Ffowcs Williams; "Large Plate Response to Finite Mach Number Boundary Layer Flow," Acoustical Fatigue in Aerospace Structures, Edited by W.J. Trapp and D.M. Forney, Syracuse University Press, 1965.

24. R.H. Lyon; "Boundary Layer Noise Response Simulation with a Sound Field," Acoustical Fatigue of Aerospace Structures, Edited by W.J. Trapp and D.M. Forney, Syracuse University Press, 1965.

25. J.F. Wilby and E.J. Richards; "Panel Response and Its Relation to the Type of Excitation," Acoustical Fatigue of Aerospace Structures, Edited by W.J. Trapp and D.M. Forney, Syracuse University Press, 1965.

26. L. Maestrello; "Measurement of Panel Response to Turbulent Boundary Layer Excitation," AIAA Journal, Febraury 1965.

27. D.J. Bozich; "Spatial Correlation in Acoustic-Structural Coupling," J. Acoust. Soc. Am., Vol. 36, No. 1, January 1964.

28. P.H. White; "Transduction of Boundary-Layer Noise by a Rectangular Panel," Paper 6B2 Presented before the 71st Meeting of the Acoustical Society of America, Boston, June 1966.

APPENDIX C

RADIATION DAMPING FOR A PANEL MOUNTED IN THE WALL OF A WIND TUNNEL

It has been observed experimentally when panels are mounted in one wall of a wind tunnel or of a progressive wave section of an acoustic testing facility that the first mode of the panel is highly damped if the ratio of the area of the panel to the duct cross-sectional area becomes appreciable.

Bozich (in Reference 18) has studied this phenomenon theoretically by considering the radiation impedance of a "modal" piston mounted in the wall of a semi-infinitely long duct of constant cross-sectional area. The result is found that the magnitude of the acoustic radiation critical damping ratio is proportional to the ratio of panel area to the duct cross-sectional area, inversely proportional to the square of panel thickness, and decreases rapidly with increasing mode number.

In the design of this experiment, it was decided that the acoustic damping experienced by the panel mounted in the wall of the wind tunnel should not exceed the range of normal structural damping. The critical damping ratio normally experienced by structure is in the range of 0.005 to 0.02. For the purposes of the analysis the wind tunnel was assumed to be a semi-infinite duct (the impedance of the fan end being assumed infinite).

For a simply-supported panel Bozich derives the following theoretical result for the acoustic radiation critical damping ratio $\delta_{r_{mn}}$:

$$\delta_{r_{mn}} = \frac{32\,\rho_o\,c}{\pi^6}\left[k_{mn}\right]\cdot\left[\frac{ab}{S_r}\right]\sqrt{\frac{12\,(1-\nu^2)}{E\,\rho}} \qquad (C\,1)$$

where k the non-dimensional parameter is given by:

$$k_{mn} = \frac{a^2\,b^2}{h^2\,m^2\,n^2\,(b^2\,m^2 + a^2\,n^2)} \qquad (C\,2)$$

and where:

a	=	length of panel
b	=	width of panel
c	=	speed of sound in air
E	=	Young's modulus of elasticity

h	=	thickness of panel
m	=	panel mode number in length direction (x-direction)
n	=	panel mode number in width direction (y-direction)
S_r	=	cross-sectional area of duct
ρ	=	density of panel
ρ_o	=	density of air
ν	=	Poisson's ratio.

For a clamped-clamped panel Bozich derives the following approximate theoretical result for the acoustic radiation critical damping ratio $\delta_{r_{11}}$ (for the first mode):

$$\delta_{r_{11}} \approx \frac{\rho_o c}{100.8} \left[k_{11}\right] \cdot \left[\frac{a\,b}{S_r}\right] \sqrt{\frac{12\,(1-\nu^2)}{E\,\rho}} \qquad \text{(C 3)}$$

where the symbols used are as defined above. It is observed that on comparing Equations (C 1) and (C 3), the acoustic damping is appreciably less for a clamped-clamped panel than for a simply-supported panel of the same dimensions. This is mainly due to the increase in frequency which results when the panel is clamped instead of simply-supported. In fact, if simply-supported and clamped-clamped panels of the same material are chosen having the same length and width, but with different thicknesses, so that their fundamental frequencies are the same, then Equations (C 1) and (C 3) show that the predicted acoustic damping is approximately the same for the two panels.

Numerical Evaluation:

Equations (C 1) and (C 3) were evaluated using the following values for a steel panel mounted in the tunnel wall:

a	=	4 in. = 1/3 ft.
b	=	8 in. = 2/3 ft.
c	=	1120 fps
E	=	4.08×10^9 lb./ft.^{2}
h	=	0.005 in. = 0.000417 ft.
m	=	1
n	=	1

$S_r = 32 \times 10 = 320$ in.^{2}

$\rho = 480$ lb./ft.^{3}

$\rho_o = 0.0766$ lb./ft.^{3}

$\nu = 0.28$

Pinned-Pinned Panel:

Using the values given above

$(ab/S_r) = 0.1$

$k_{11} = 0.512 \times 10$ [from Equation (C 2)]

and thus from Equation (C 1):

$\delta_{r_{11}} = 0.0613$

Clamped-Clamped Panel:

Again using the above values from Equation (C 3)

$\delta_{r_{11}} = 0.01825.$

The value of acoustic damping calculated for a clamped-clamped panel was thought to be acceptable since it is within the range of structural damping (0.005 to 0.02) discussed above. Thus it was decided to make the test panel 4 by 8 by 0.005 in. in dimensions.

Figure 1. View of Working Section of Wind Tunnel, Showing Bell Mouth Intake, Multitube Manometer and Adjustable Separated Flow Working Section Installed.

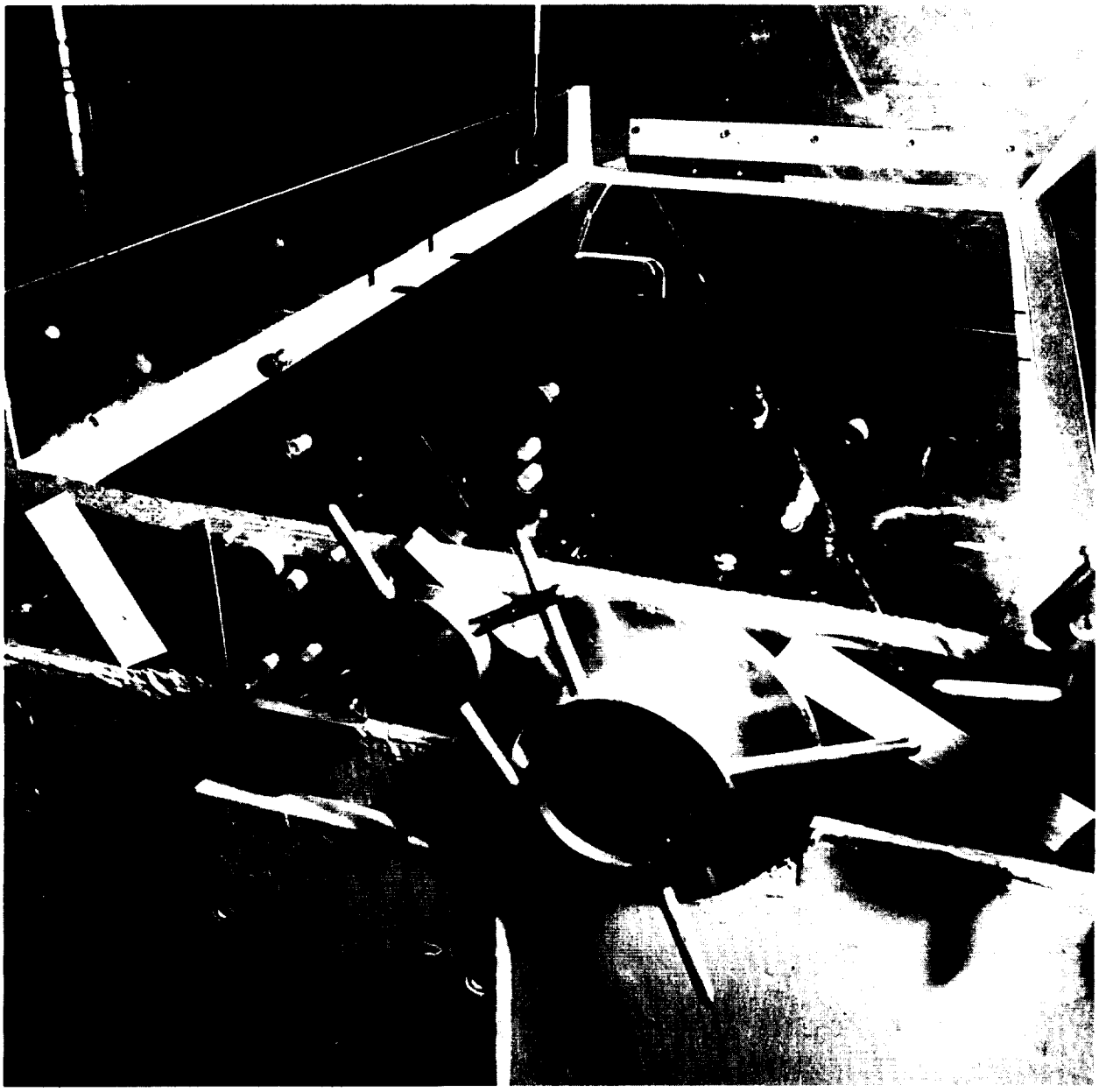

Figure 2. Adjustable Separated Flow Working Section, Showing Reverse Flow Boundary-Layer Pitot Tube and Pitch and Yaw Sensitive Pitot Tube and Also Pressure Equalization Box.

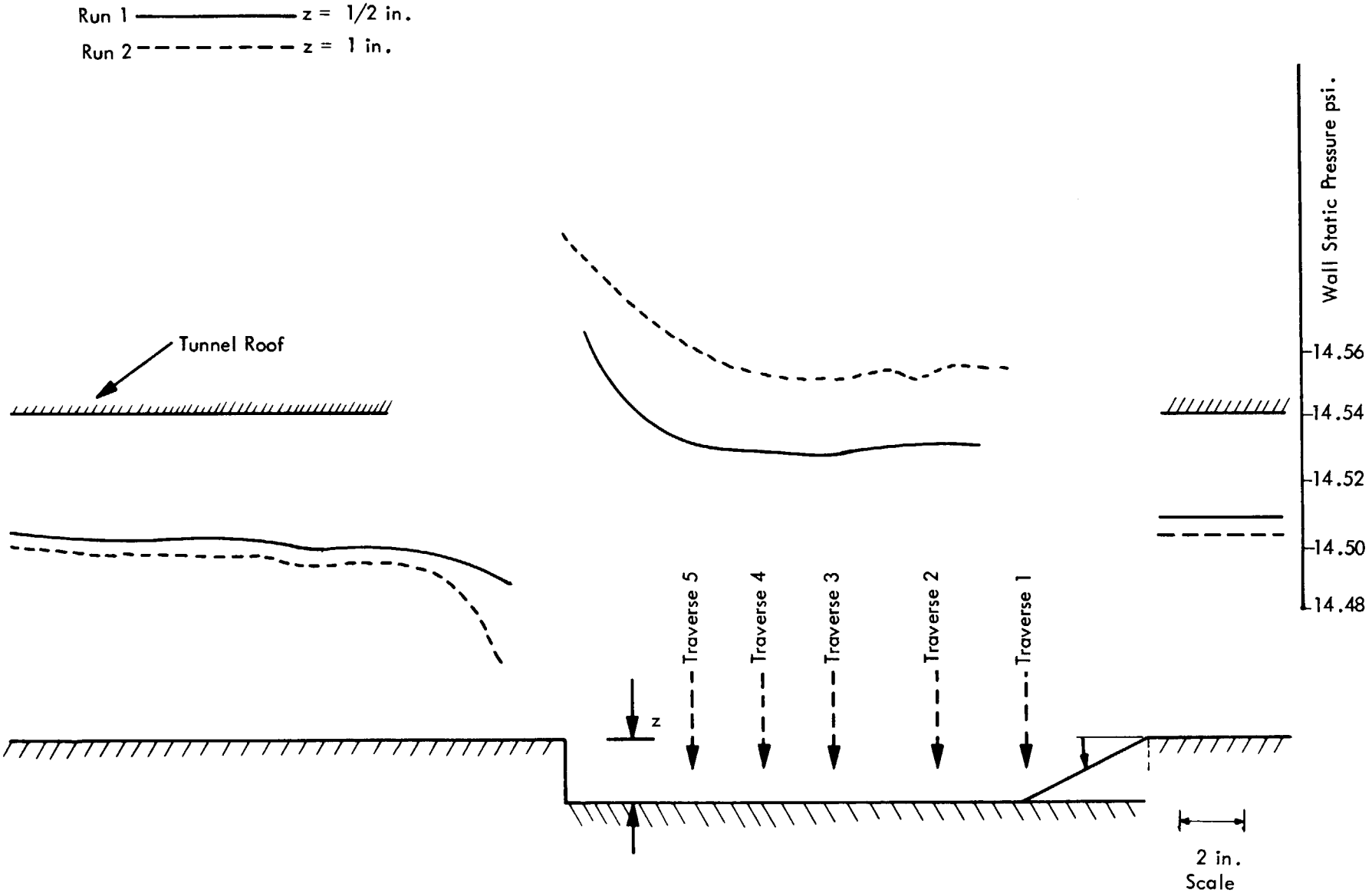

Figure 3. Wall Static Pressure Pattern for Two Different Separated Flow Floor Depths, z.

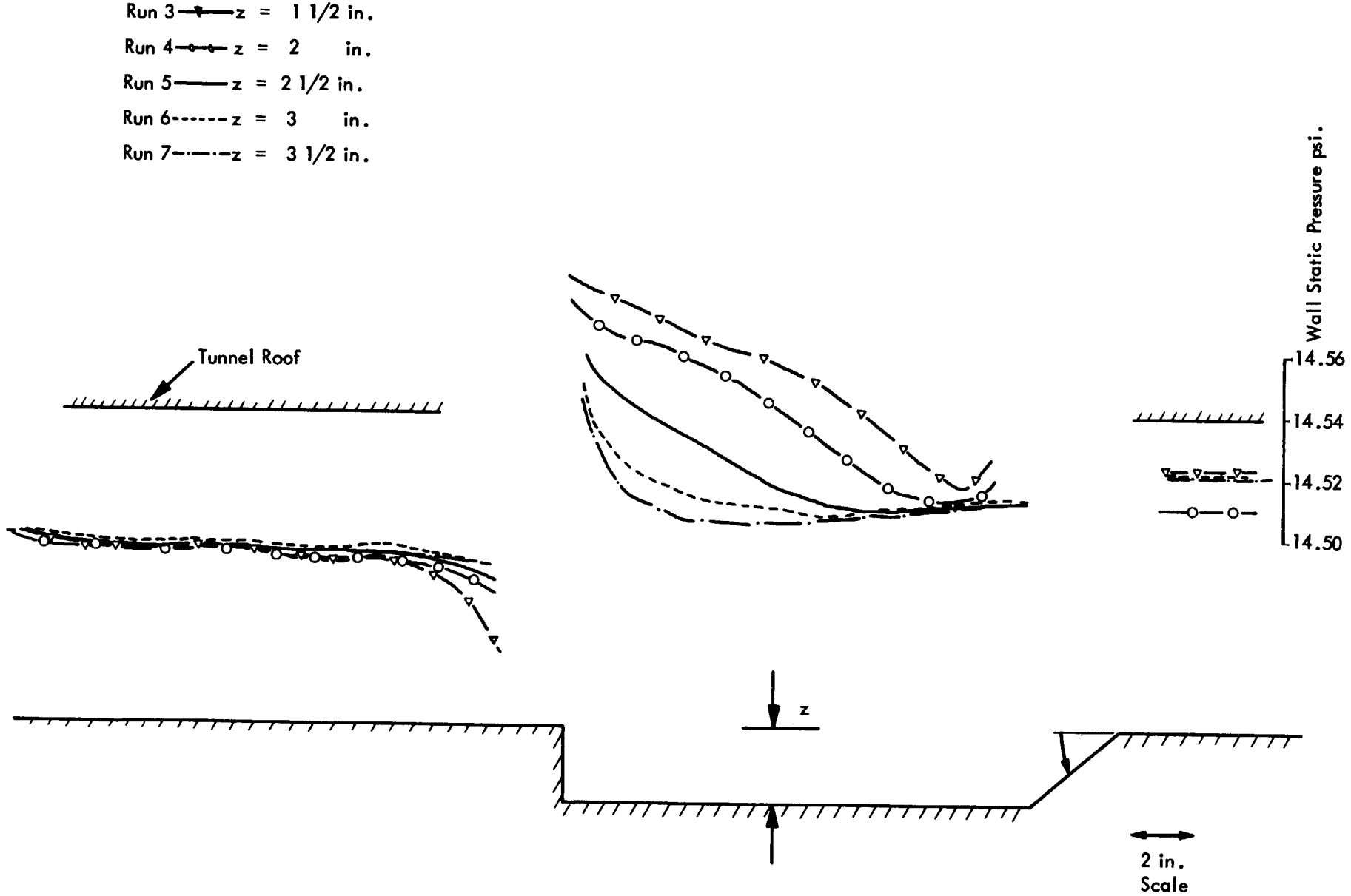

Figure 4. Wall Static Pressure Pattern for Five Further Different Separated Flow Floor Depths, z.

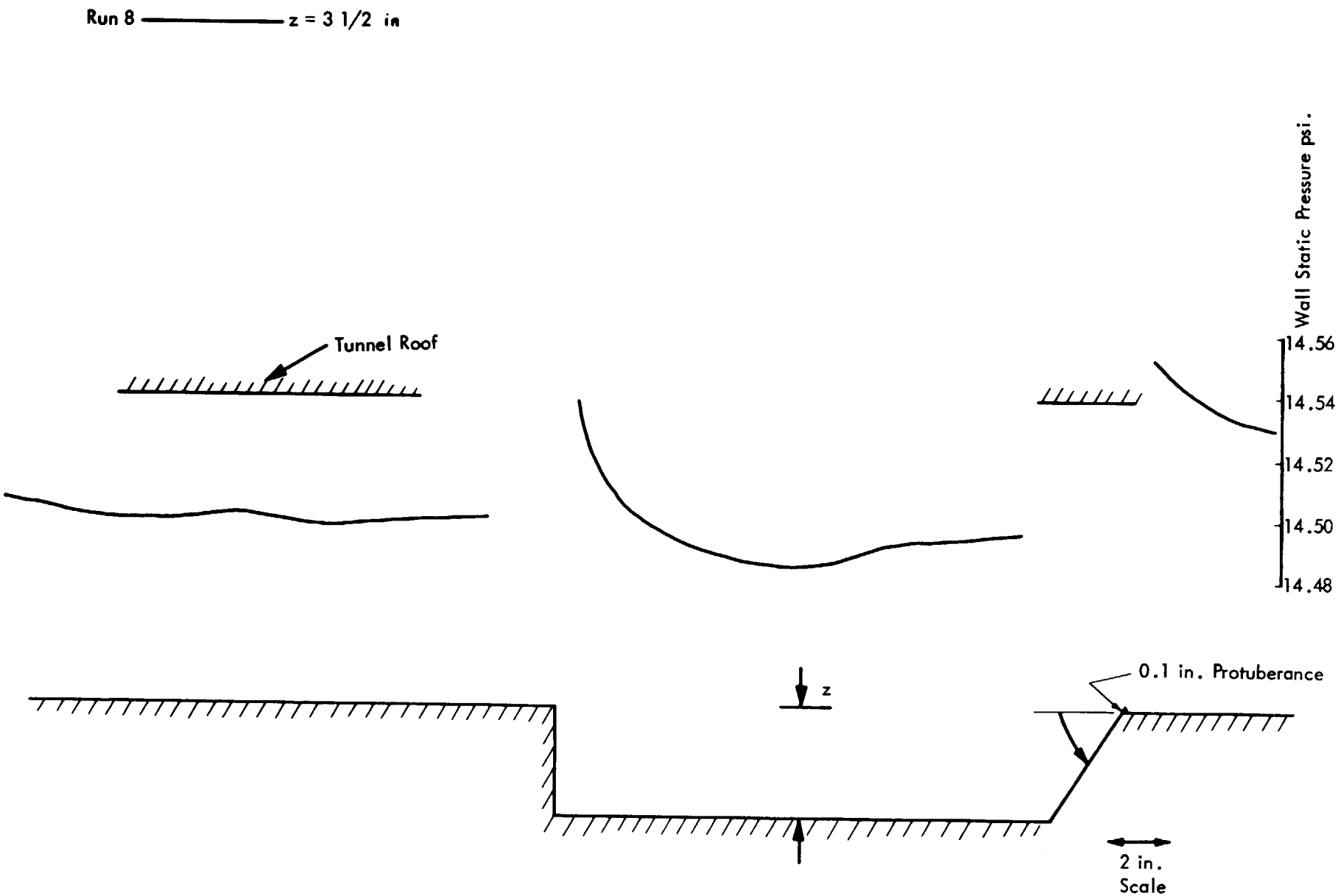

Figure 5. Wall Static Pressure Pattern for Separated Flow Floor Depth z = 3 1/2 in. and With Initial Protuberance.

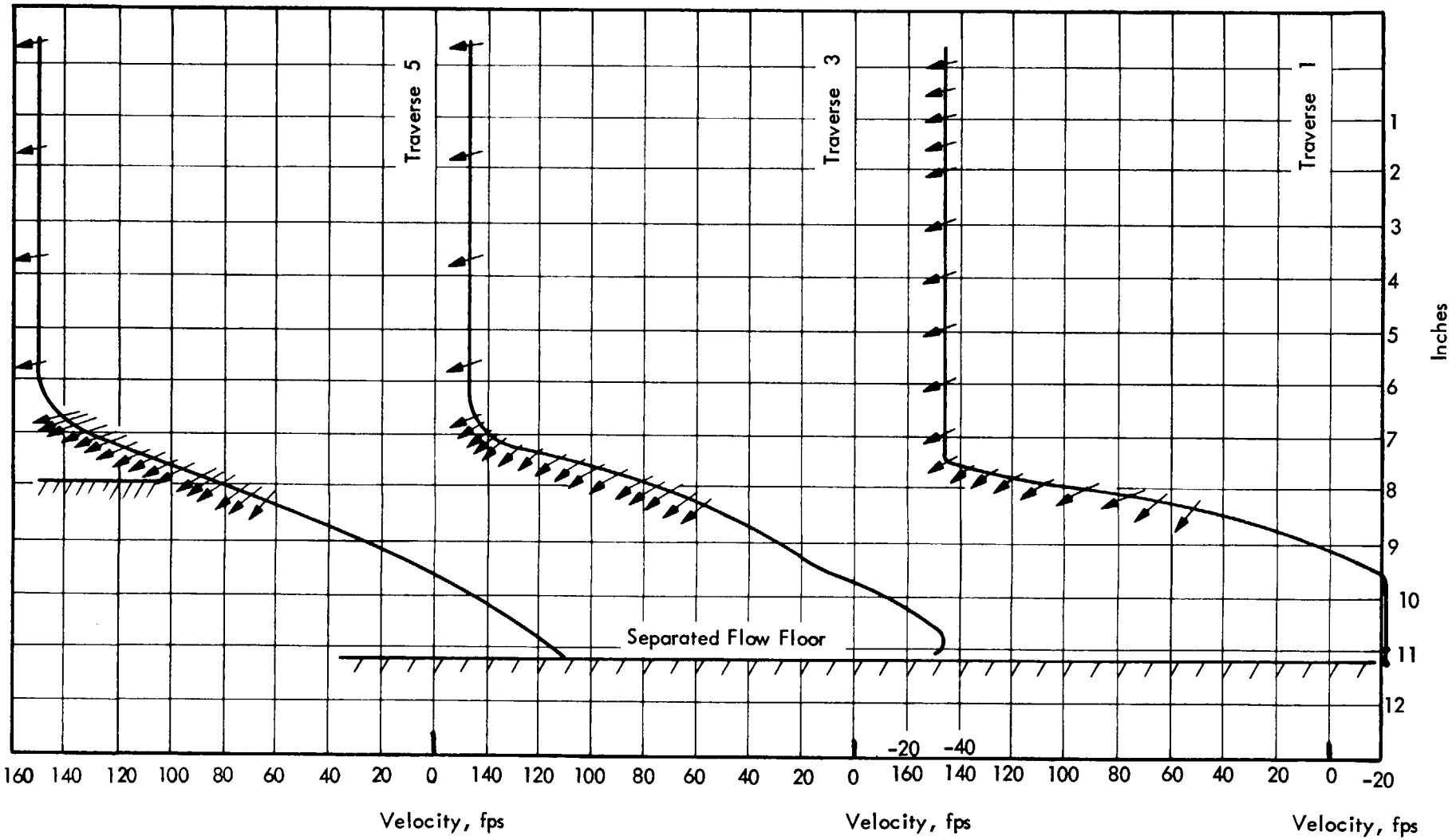

Figure 6. Velocity Traverses in Separated Flow Section.

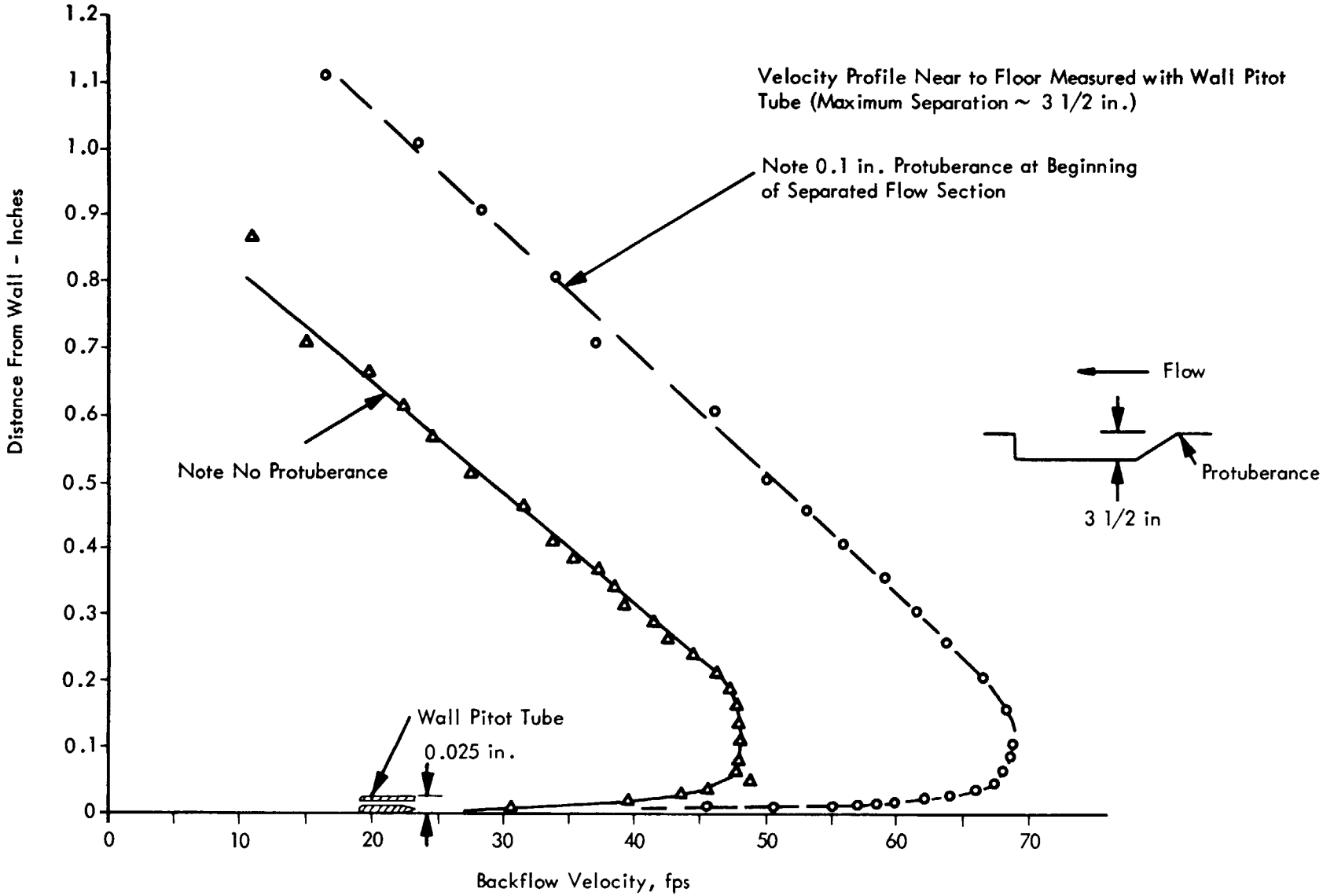

Figure 7. Velocity Profile of Reversed Flow at Station 5 Near to Floor of Separated Flow Section, With and Without Initial Protuberance.

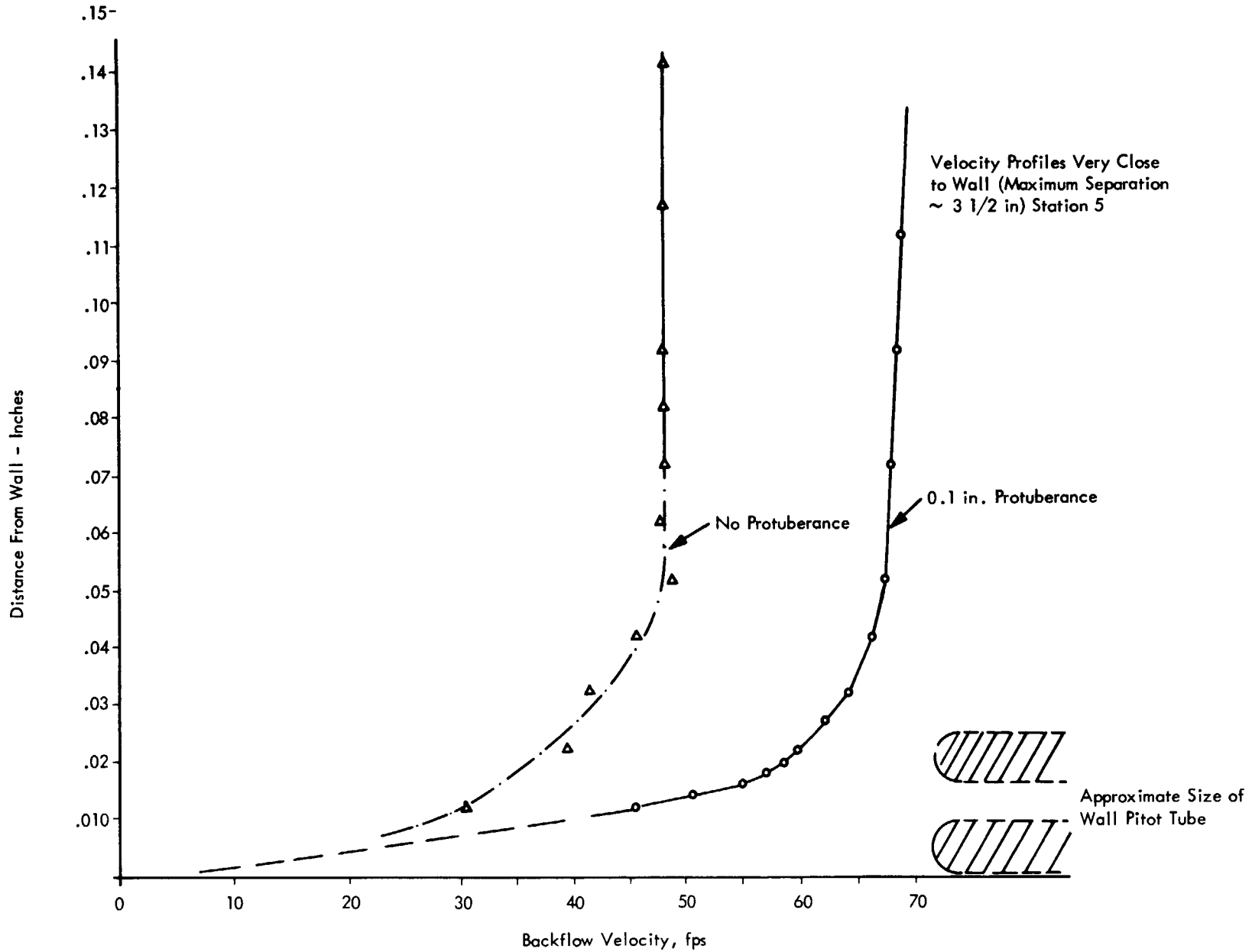

Figure 8. Velocity Profile of Reversed Flow at Station 5, Very Close to Floor of Separated Flow Section, With and Without Initial Protuberance

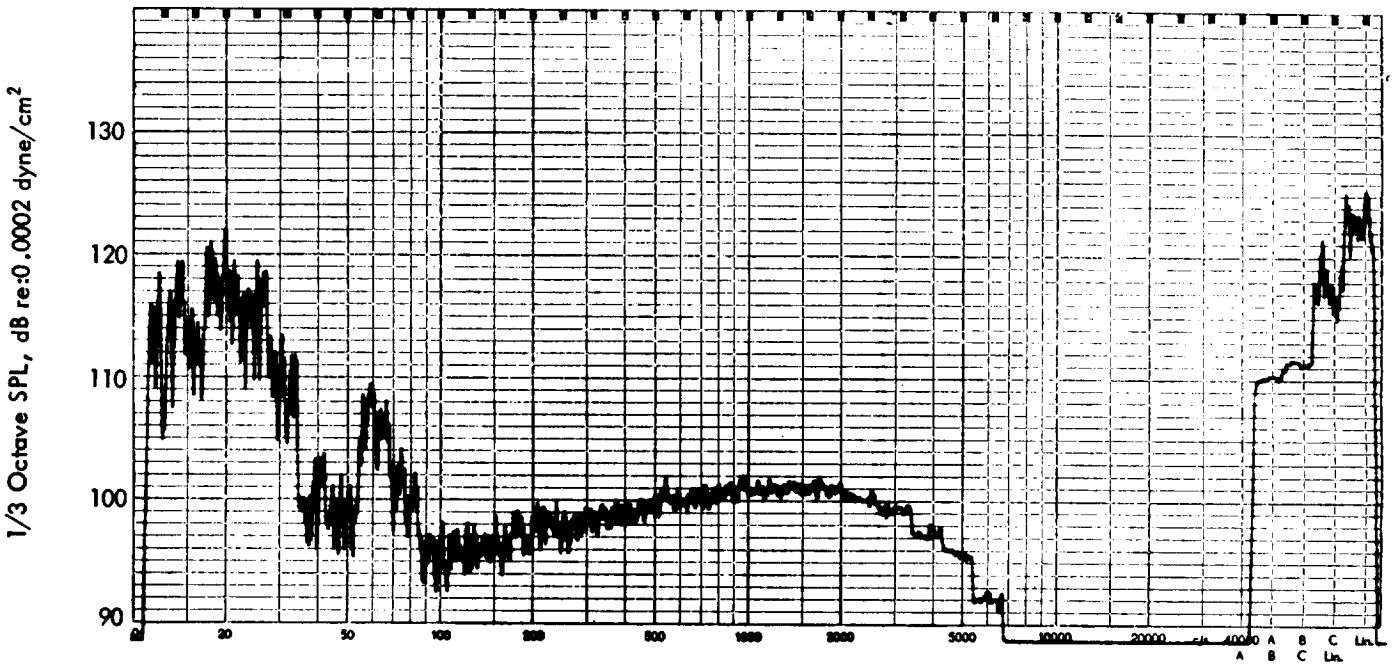

Figure 9. Third Octave Levels of Wall Pressure Fluctuations Measured for Attached Turbulent Boundary Layer with 1/4 in. Microphone at Center of Working Section (U_o = 144 fps).

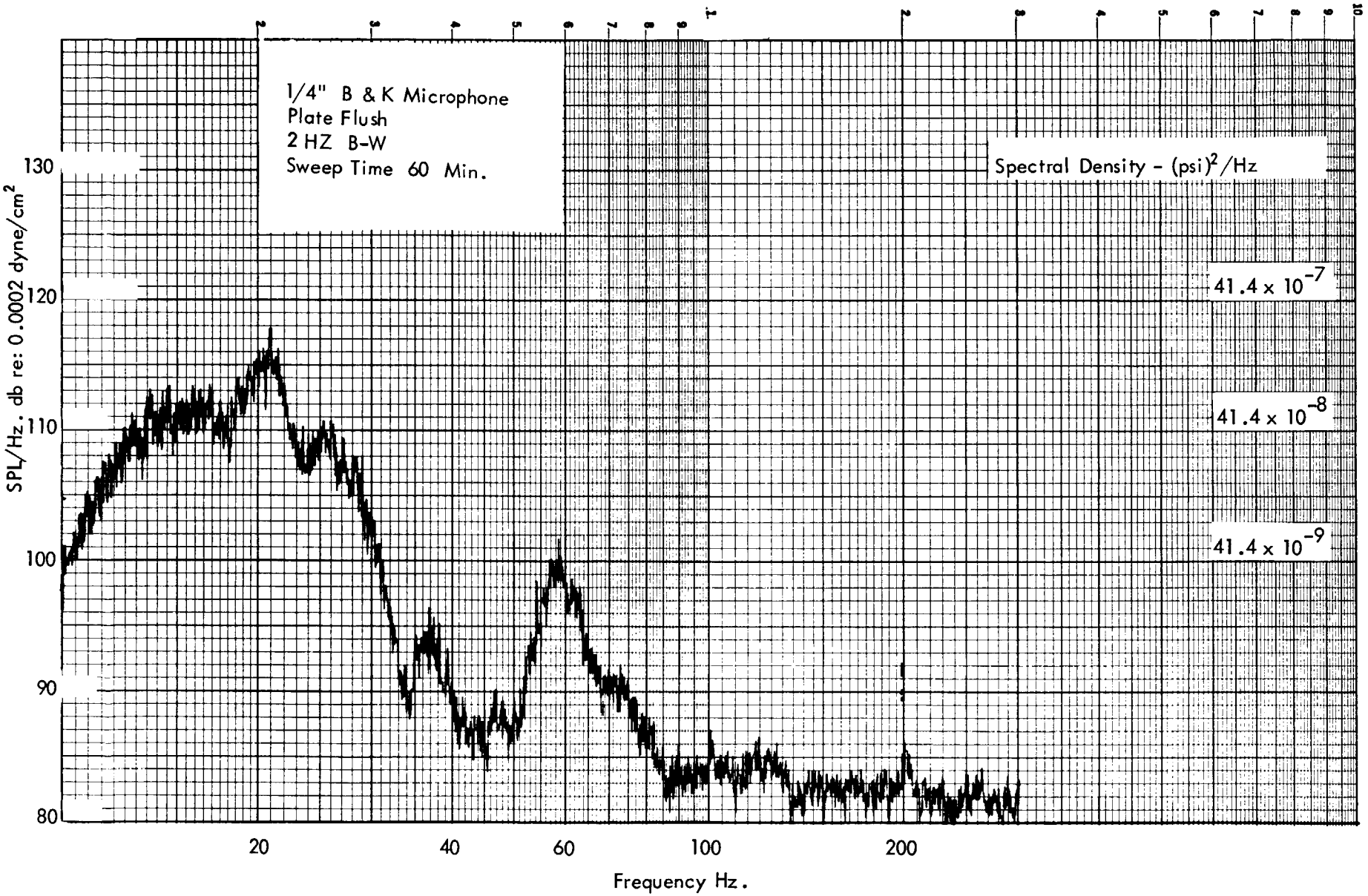

Figure 10. Narrow Band (2 Hz. Band-Width) Analysis of Wall Pressure Fluctuations Measured for Attached Turbulent Boundary Layer With 1/4 in. Microphone at Center of Working Section (U_o = 144 fps).

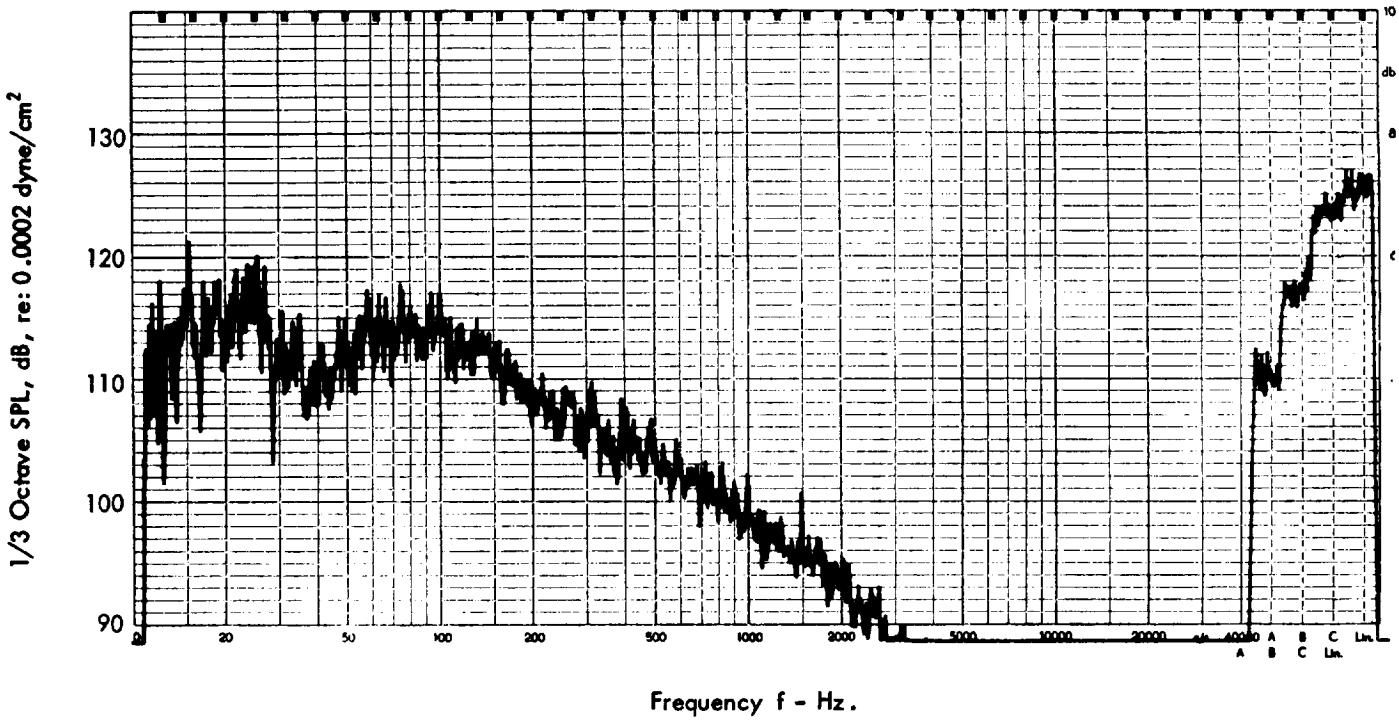

Figure 11. Third Octave Levels of Wall Pressure Fluctuations Measured for Separated Turbulent Boundary Layer (z = 3 1/2 in.) with 1/4 in. Microphone at Center of Separated Flow Section Floor (U_o = 144 fps).

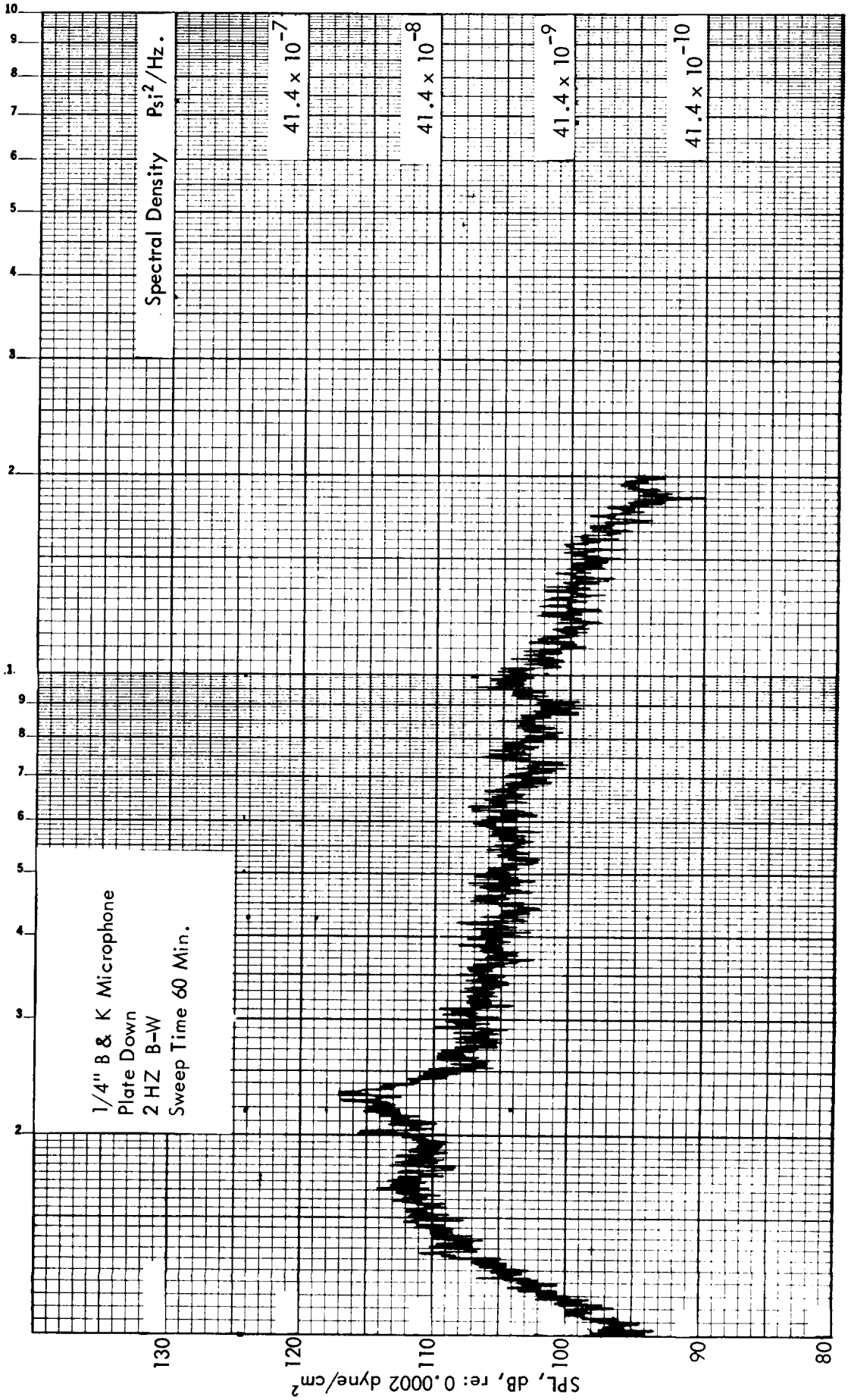

Figure 12. Narrow Band (2 Hz. Band-Width) Analysis of Wall Pressure Fluctuations Measured for Separated Turbulent Boundary Layer ($z = 3\ 1/2$ in.) with 1/4 in. Microphone at Center of Separated Flow Section Floor ($U_o = 144$ fps).

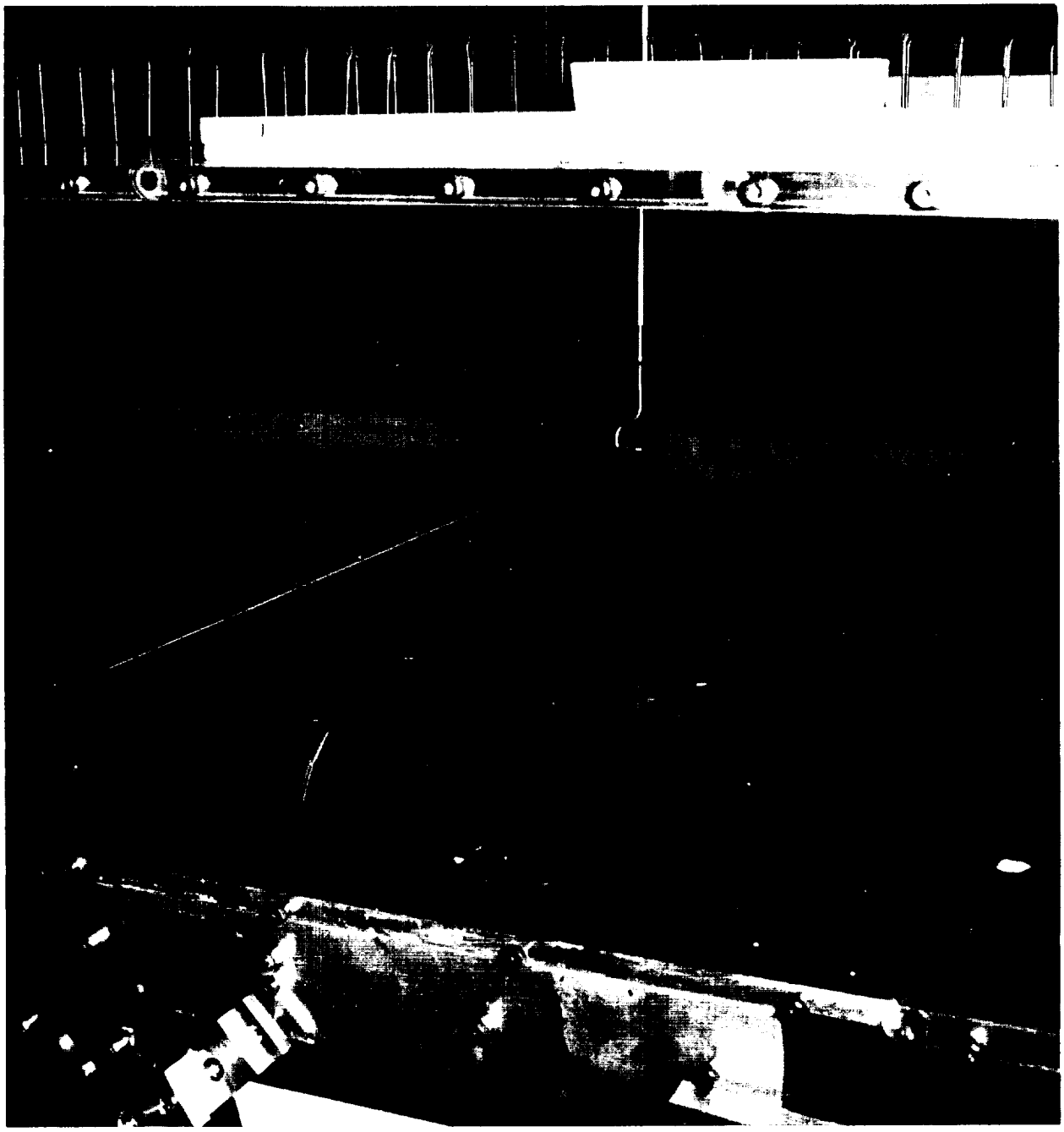

Figure 13. Four in. by 8 in. by 0.005 in. Steel Panel Mounted in 18 1/2 in. by 32 in. by 3/8 in. Stiffened Aluminum Panel Mount in Working Section of Tunnel.

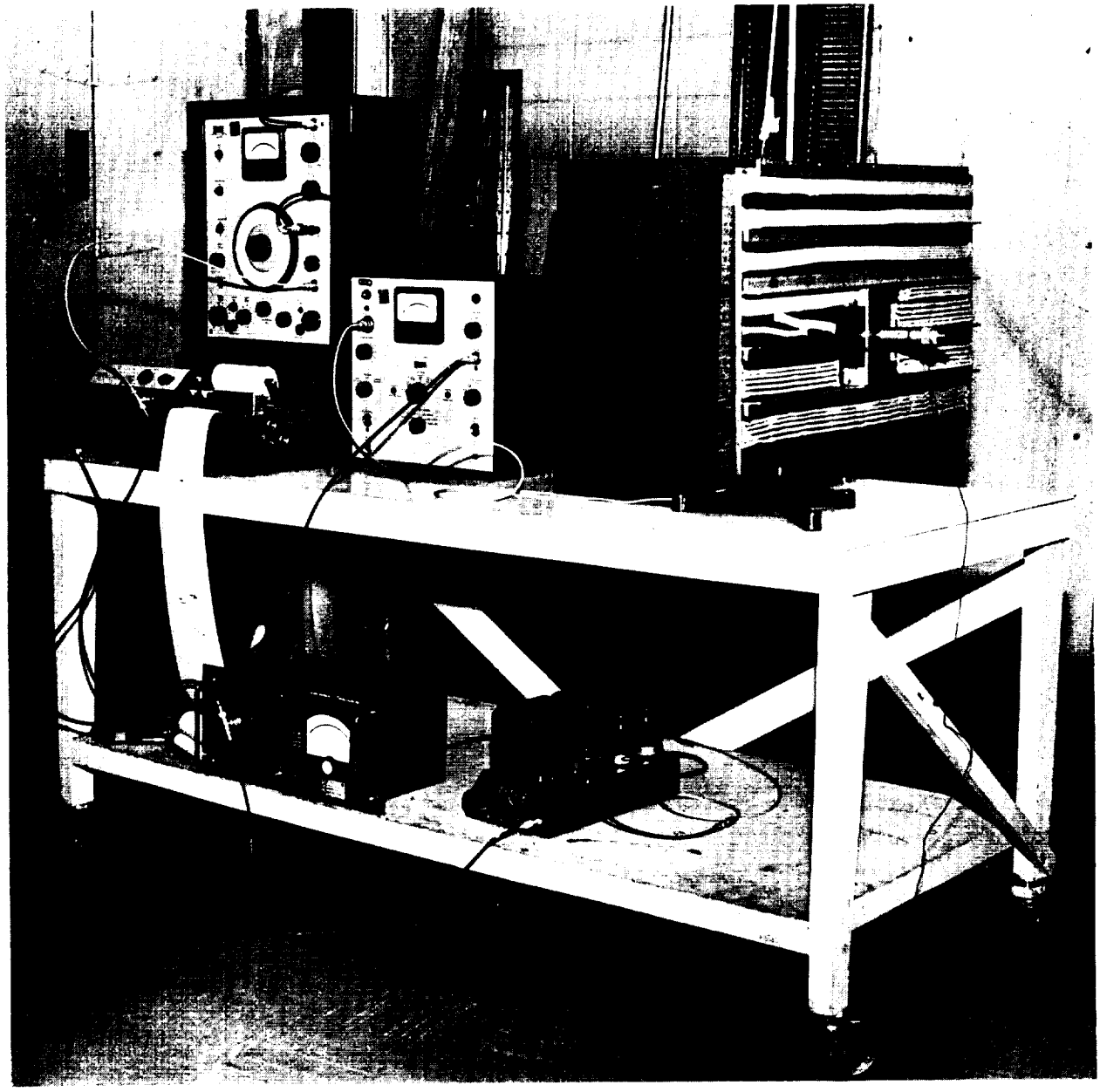

Figure 14. Steel Panel Mounted in Aluminum Panel Mount (Showing L-Section Stiffeners). Panel Undergoing Normal Incidence Acoustic Test to Determine Resonance Frequencies.

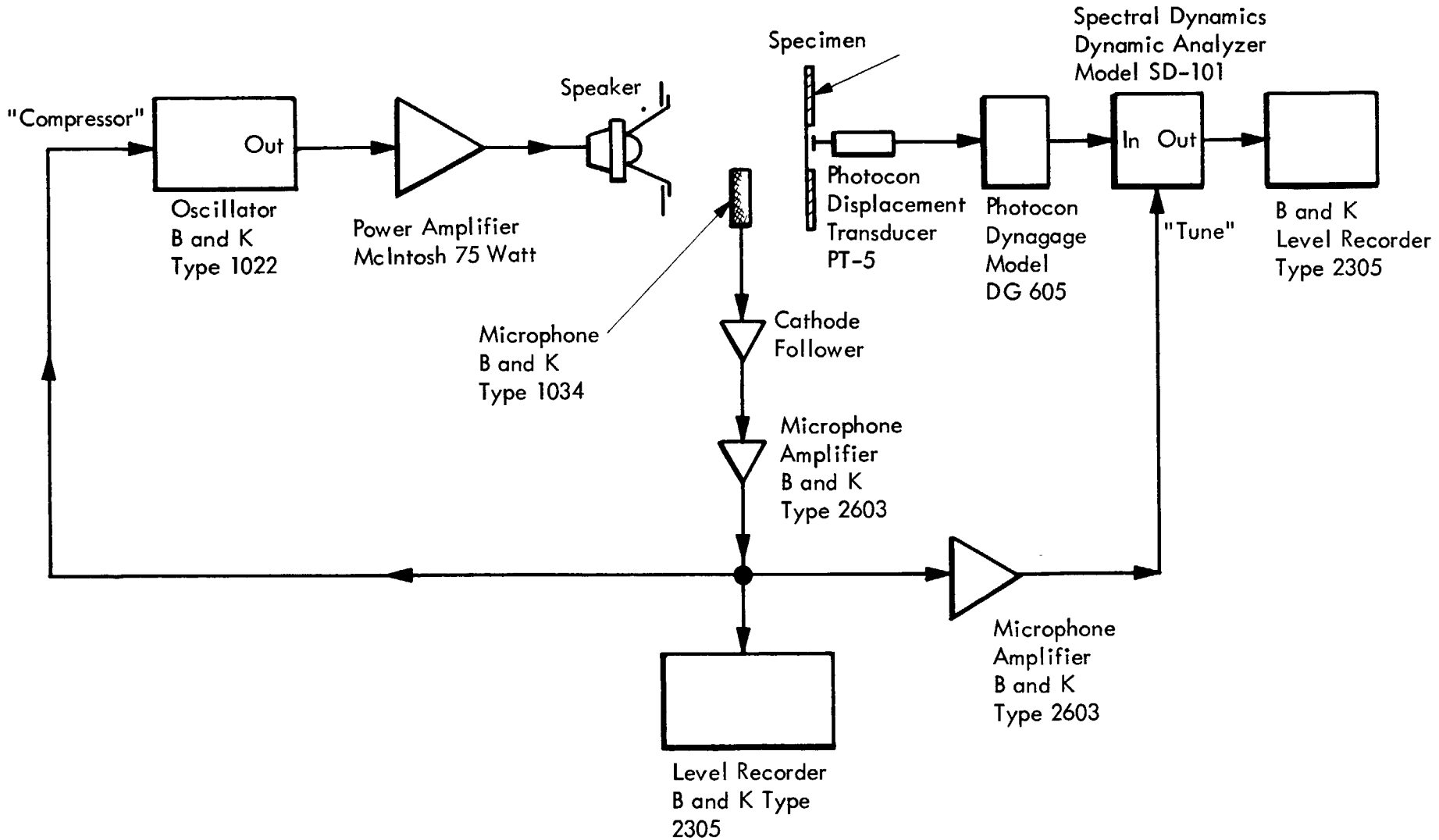

Figure 15. Block Diagram of Electronic Apparatus Used to Measure Resonance Frequencies of Steel Panel Using Loudspeaker and Capacitance Pick-up.

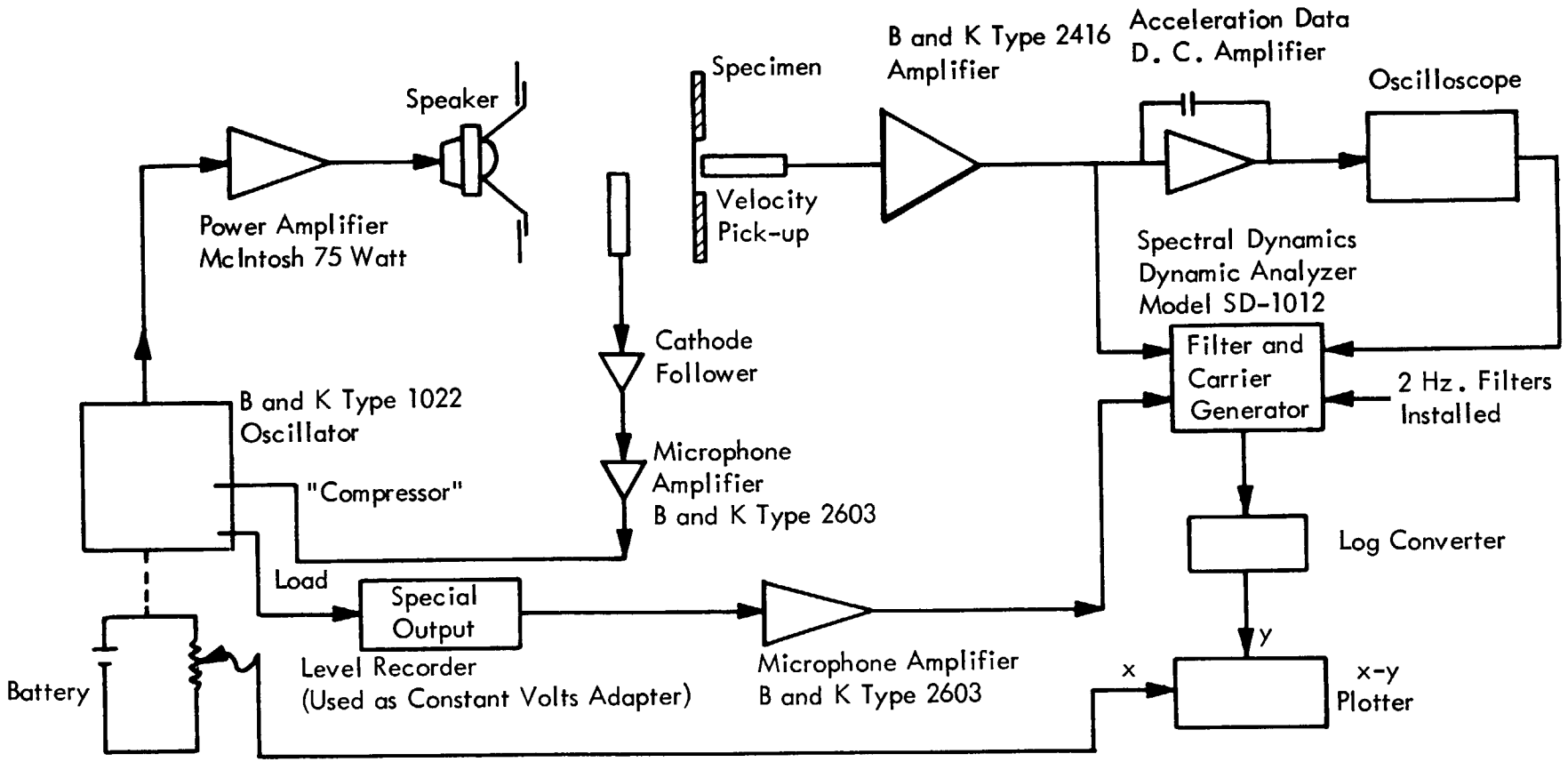

Figure 16. Block Diagram of Electronic Apparatus Used to Measure Resonance Frequencies of Steel Panel Using Loudspeaker and Wyle Velocity Pick-up.

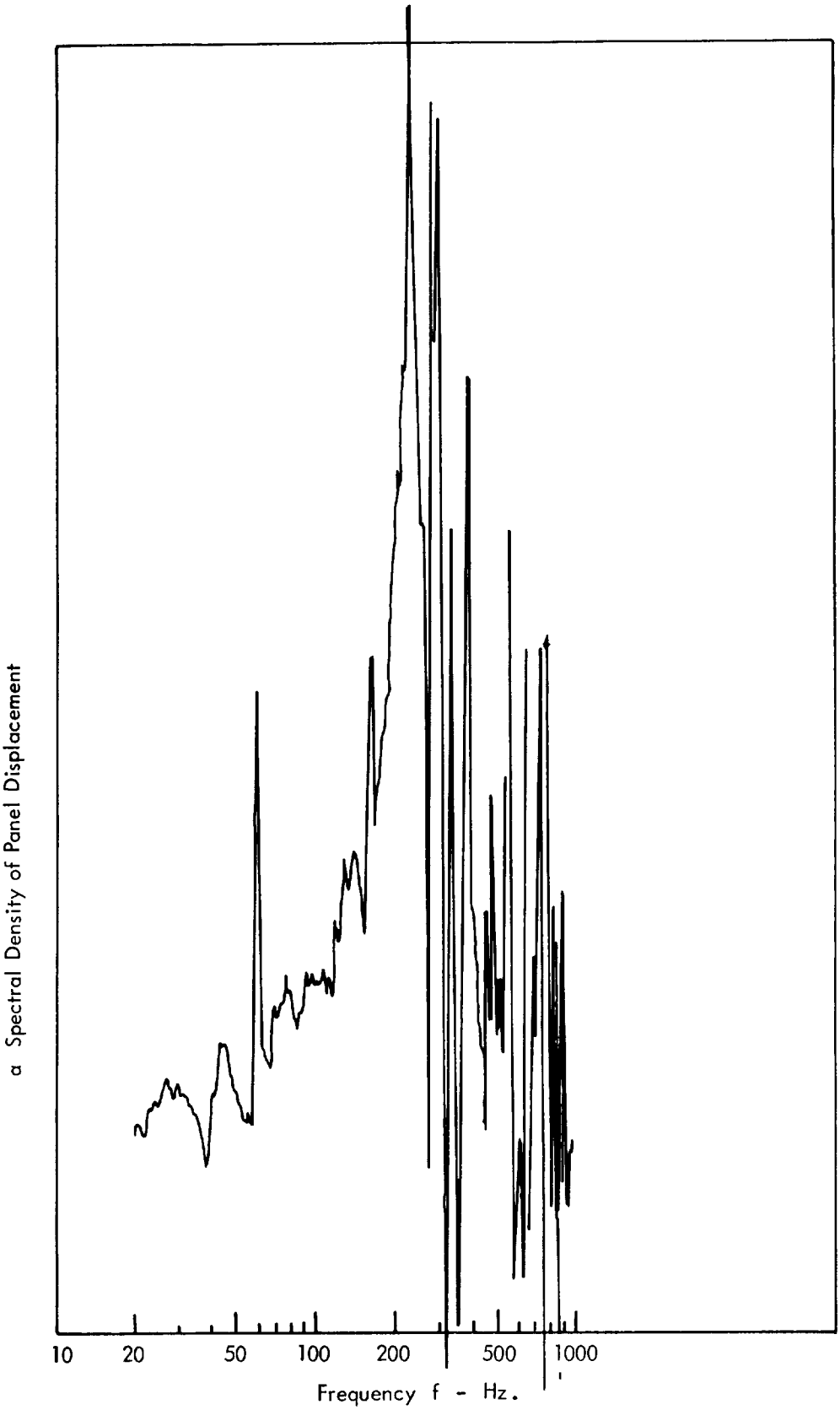

Figure 17. Spectral Density (2 Hz. Bandwidth) of Panel Displacement at Panel Center of Panel Subjected to Acoustic Waves Arriving at Normal Incidence.

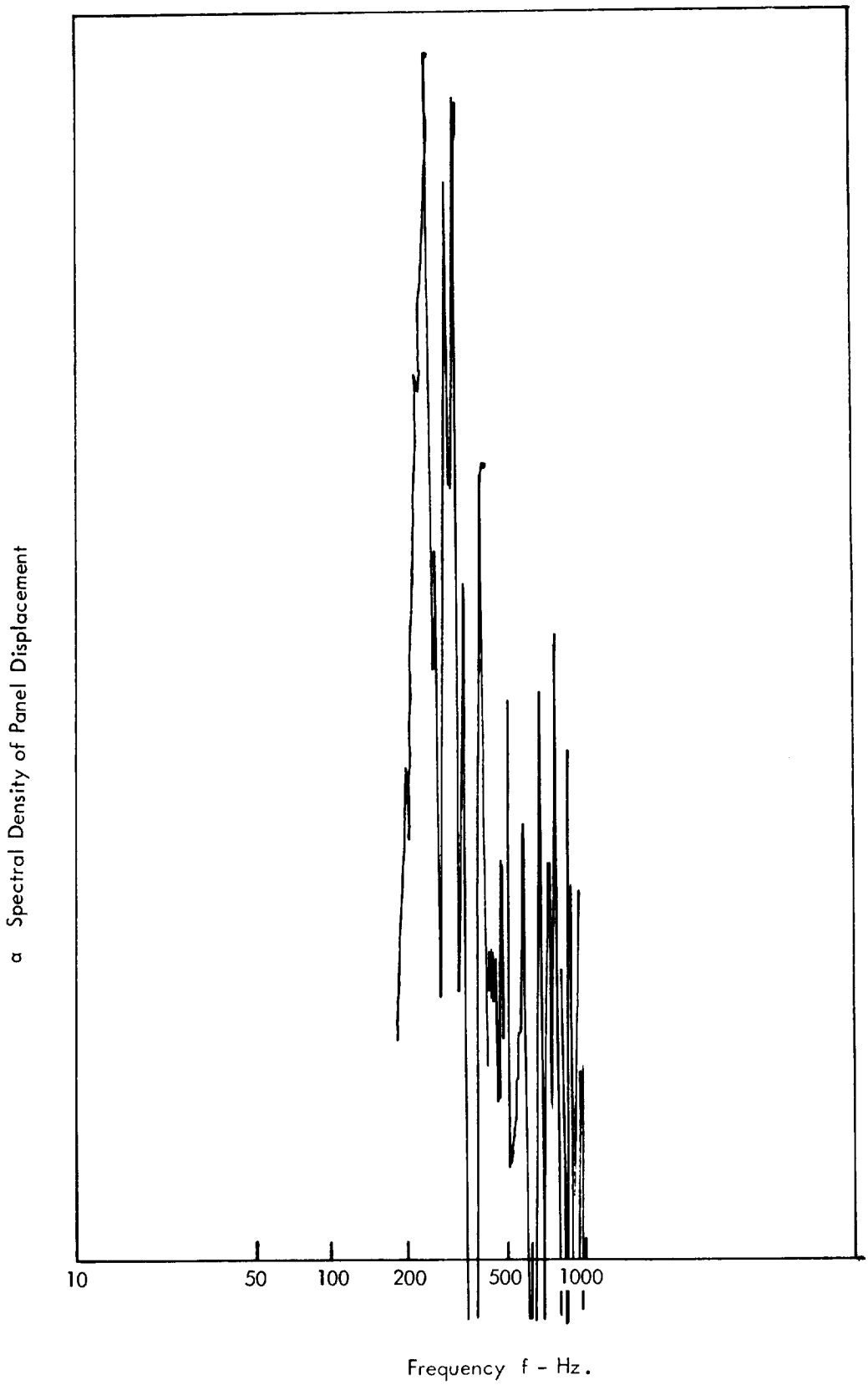

Figure 18. Spectral Density (2 Hz. Bandwidth) of Panel Displacement at Panel Center of Panel Subjected to Acoustic Waves Arriving at Grazing Incidence.

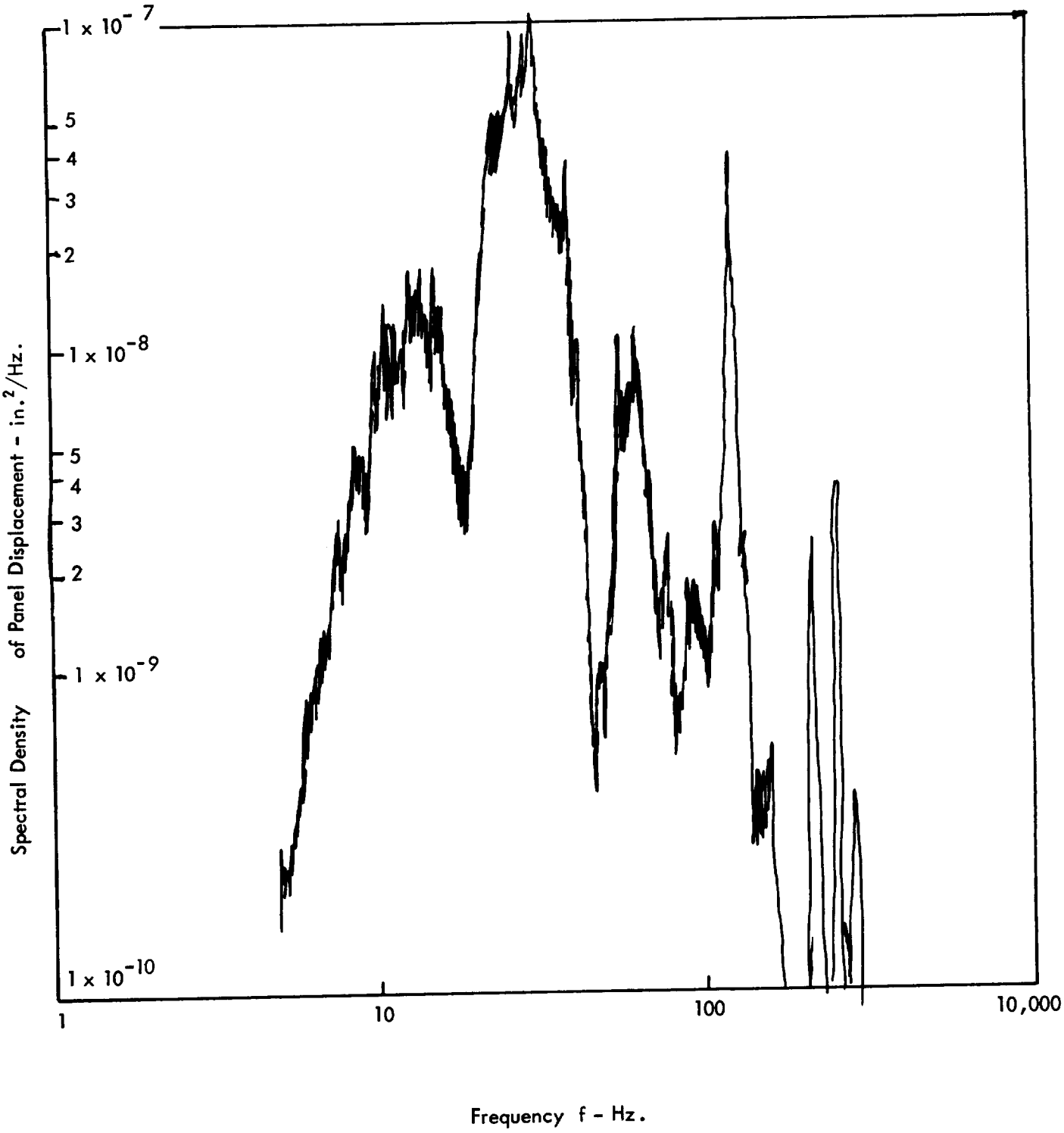

Figure 19. Spectral Density (2 Hz. Bandwidth Measurement) of Displacement of Center of Panel Subjected to Attached Turbulent Boundary Layer Pressure Fluctuations Measured with Capacitance Pick-up. (U_o = 144 fps).

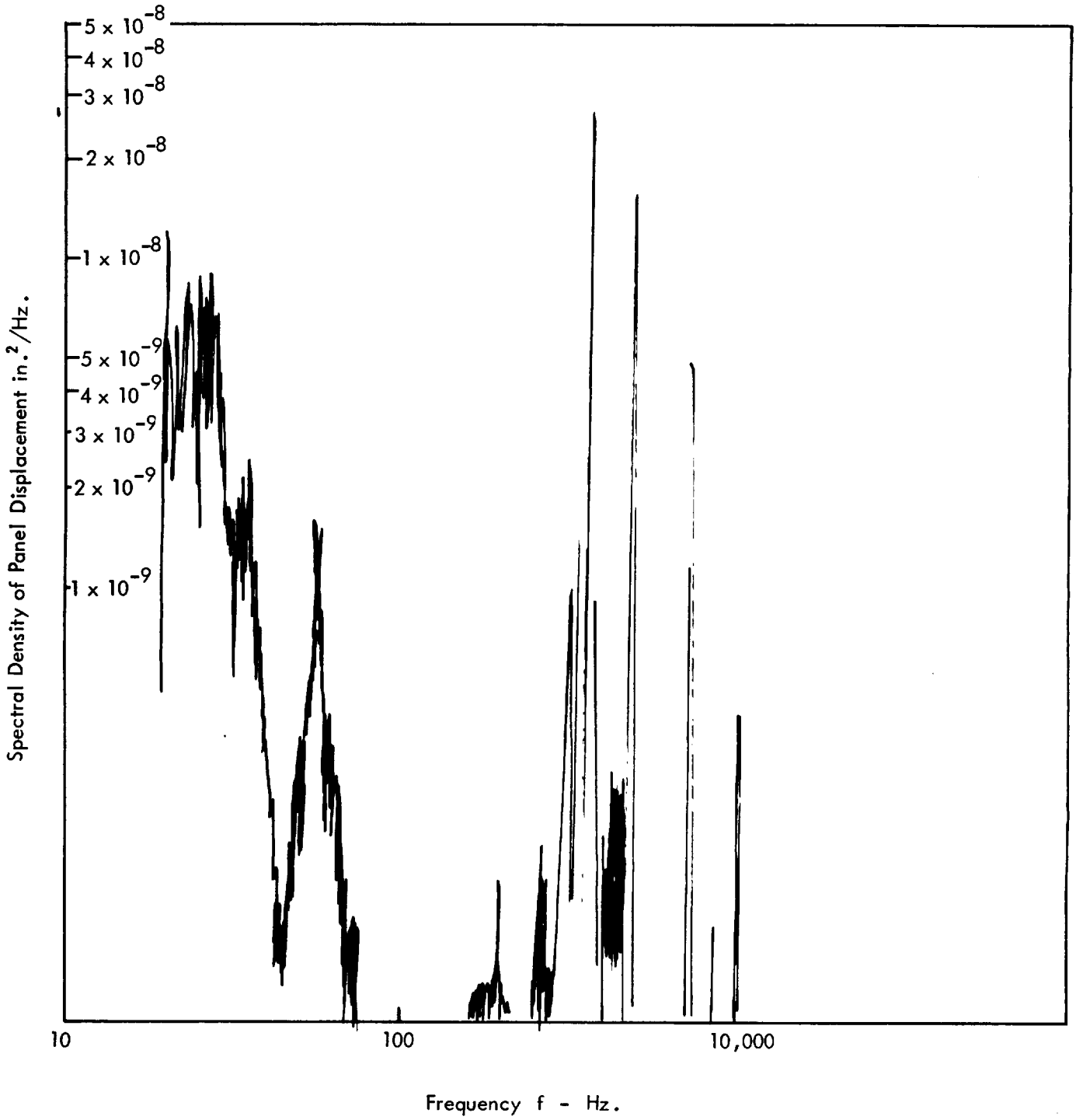

Figure 20. Spectral Density (2 Hz. Bandwidth Measurement) of Displacement of Center of Panel Subjected to Attached Turbulent Boundary Layer Pressure Fluctuations Measured with Wyle Velocity Pick-up. (U_o = 144 fps)

M = 0.52. Center Frequency Hz: 1200; 2400; 3600; 4800; 6000
(Reference 5)

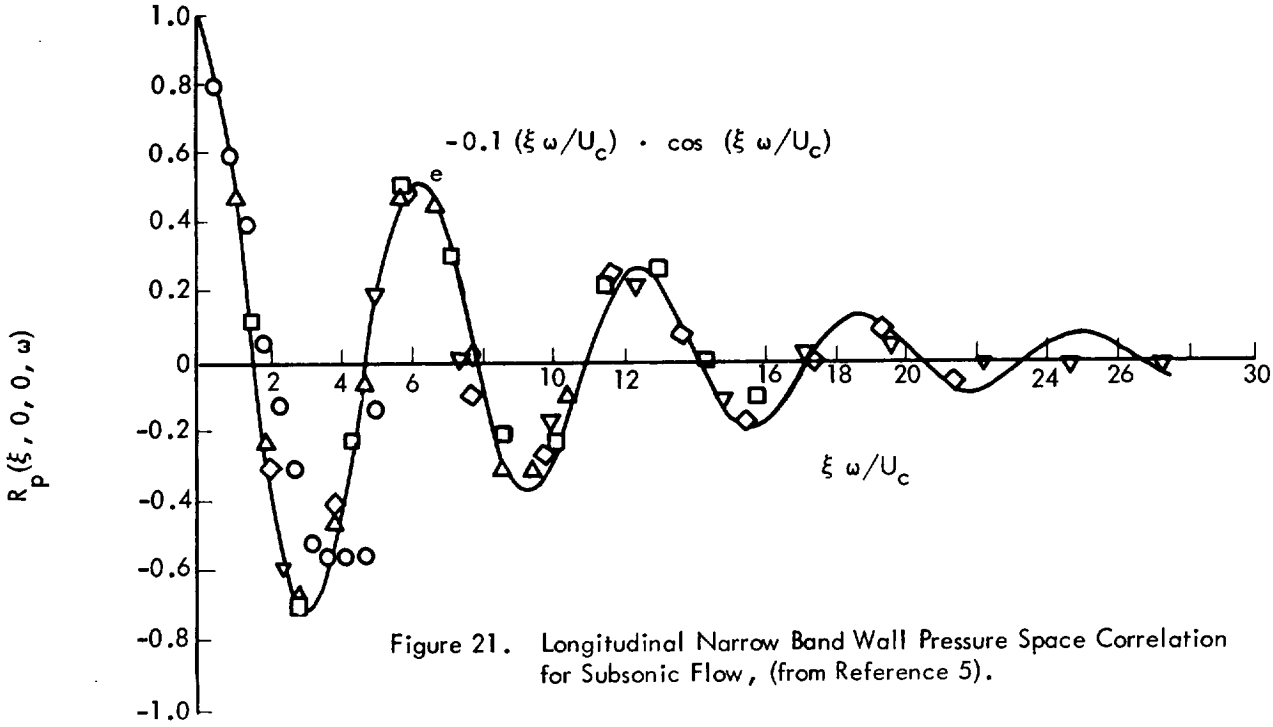

Figure 21. Longitudinal Narrow Band Wall Pressure Space Correlation for Subsonic Flow, (from Reference 5).

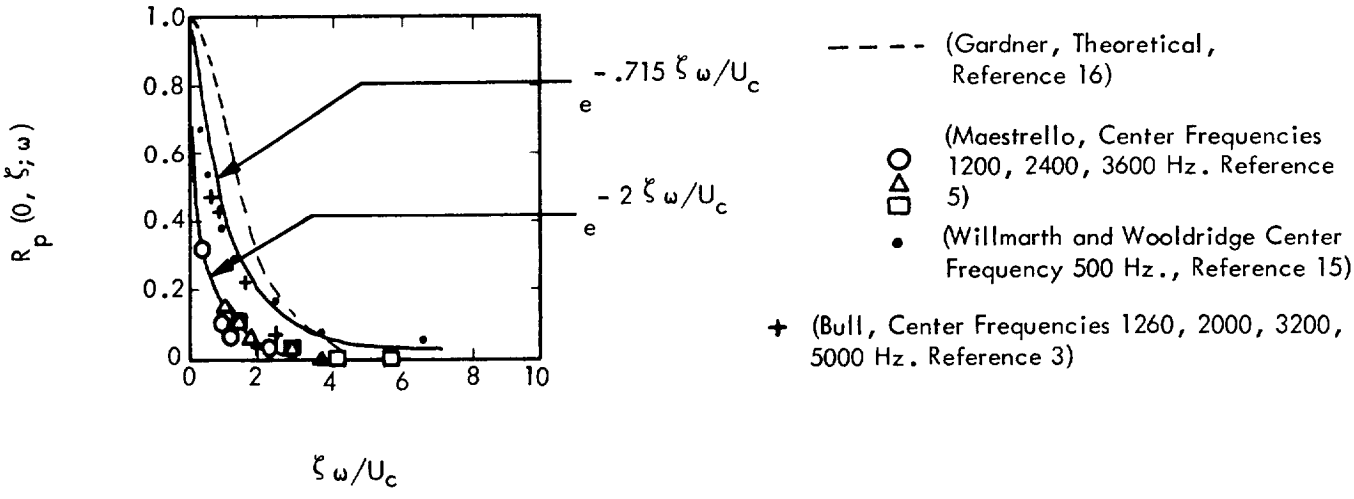

Figure 22. Lateral Narrow Band Wall Pressure Space Correlation for Subsonic Flow (from References 3, 5, and 15).

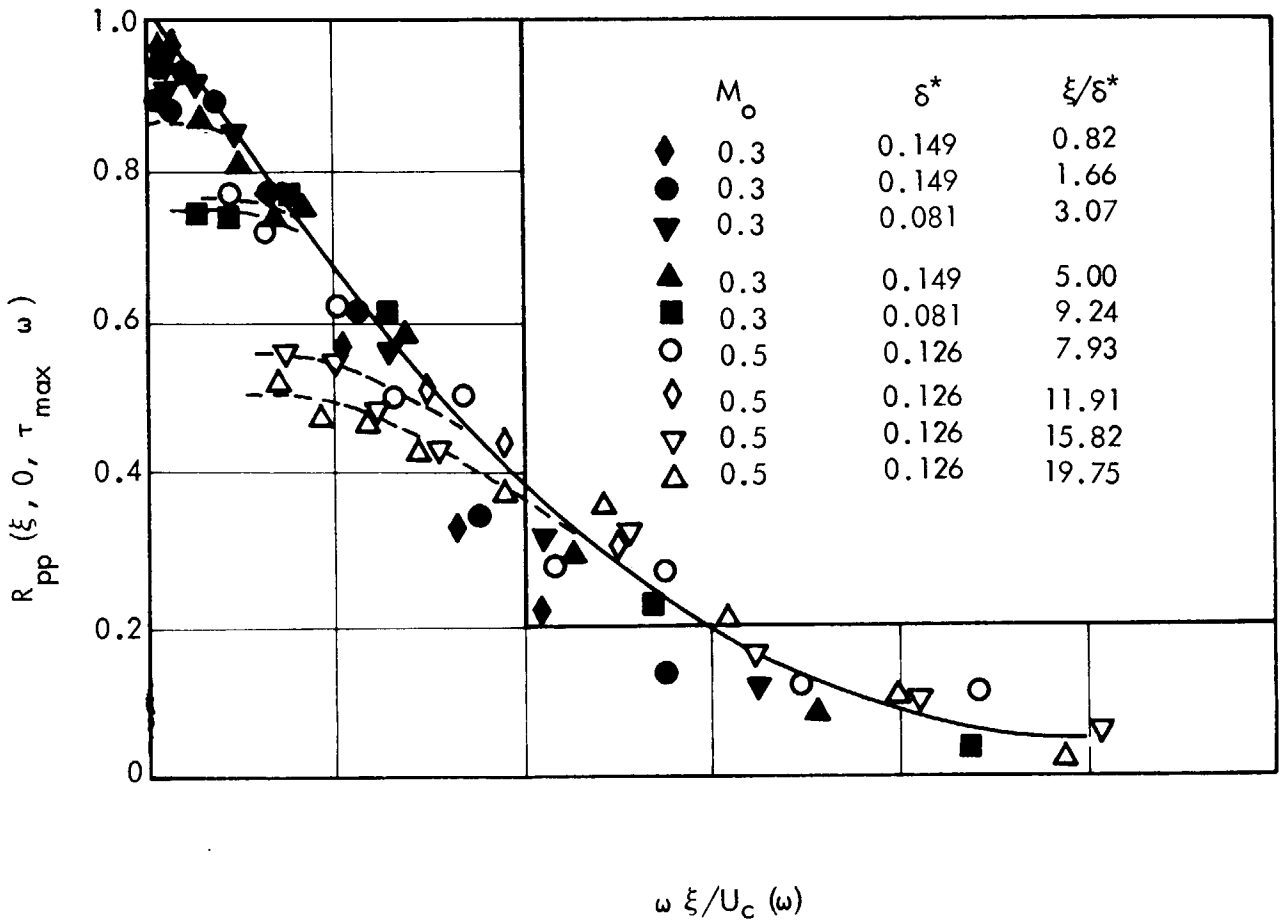

Figure 23. Amplitude of Narrow Band Longitudinal Space Time Correlations of the wall Pressure Field, (From Reference 3)

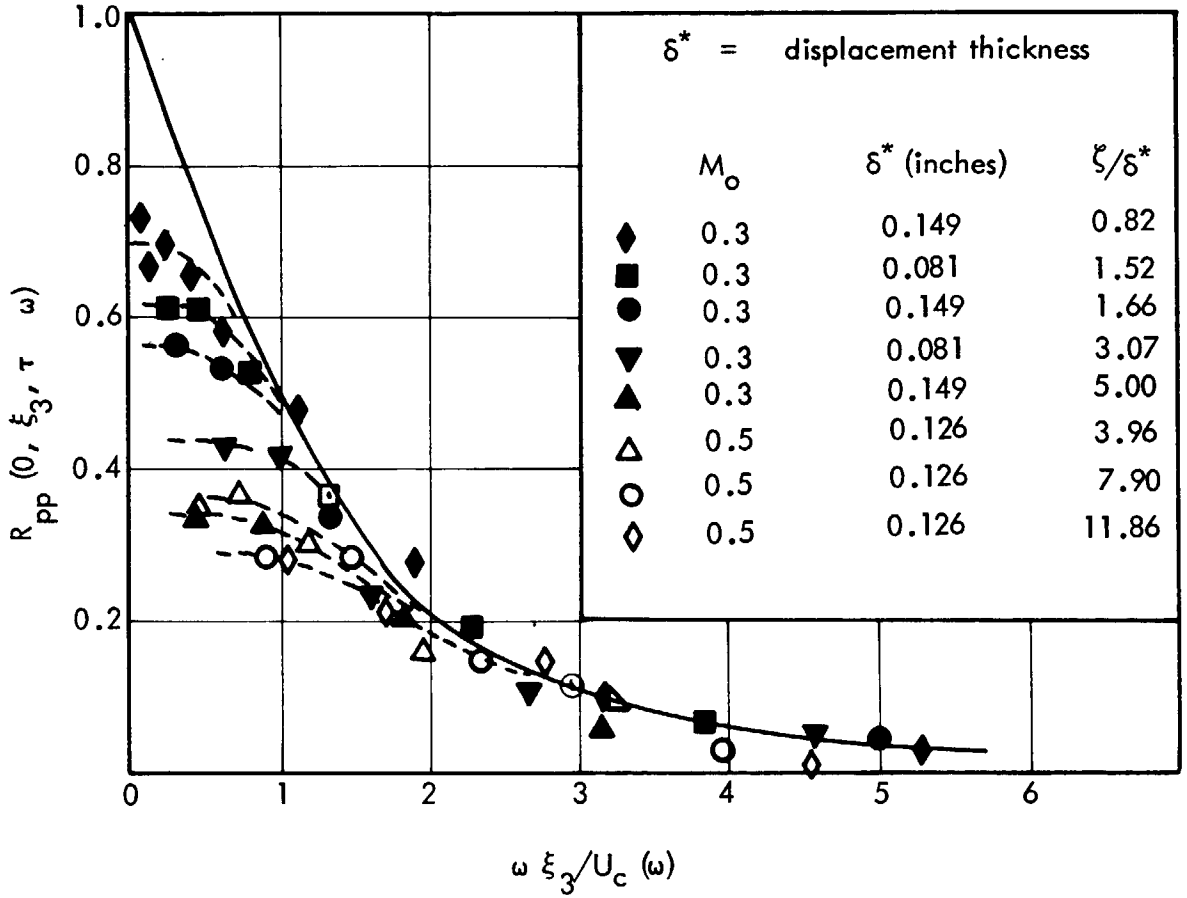

Figure 24. Amplitude of Narrow Band Lateral Space-Time Correlation of the Wall Pressure Field (from Reference 3).

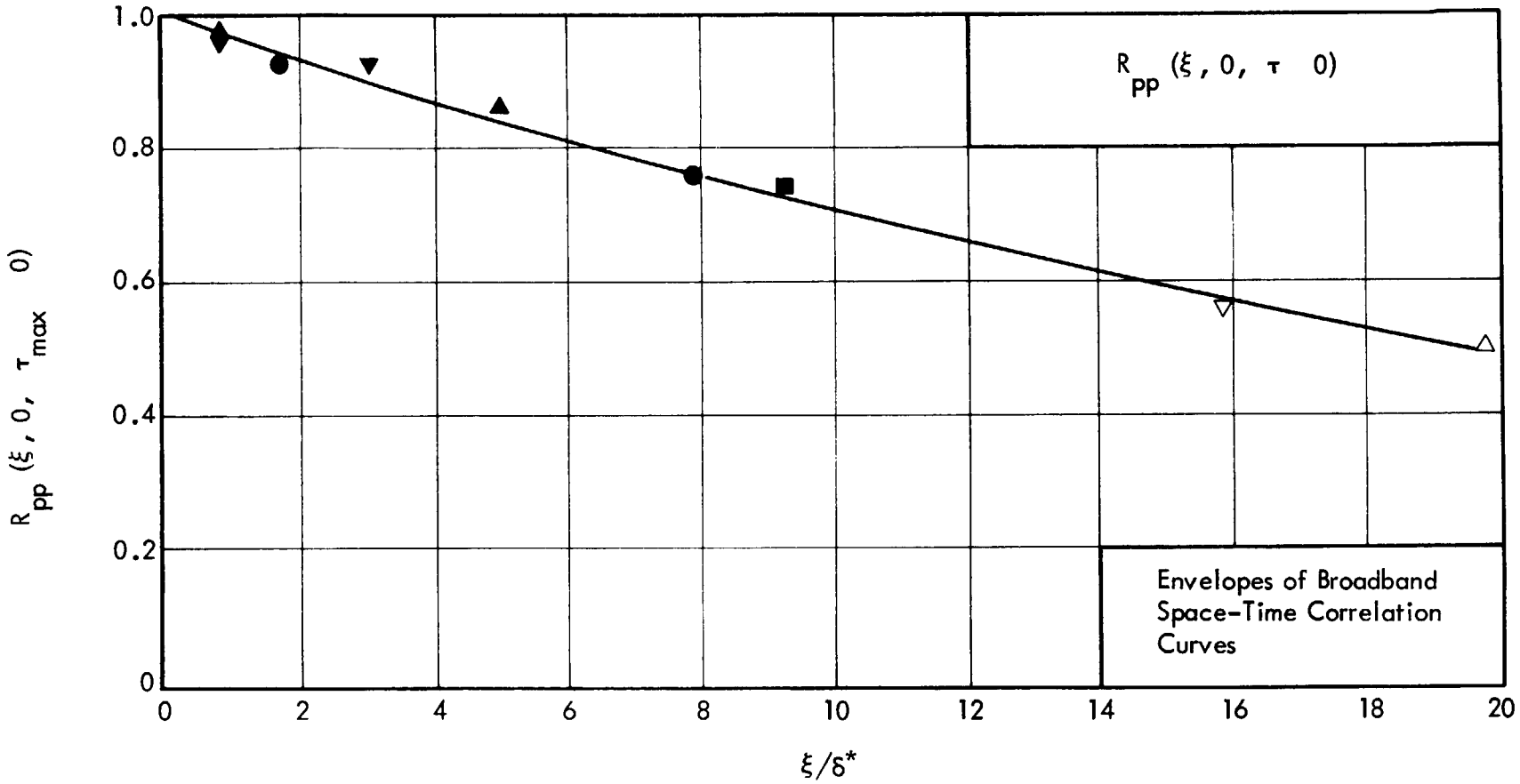

Figure 25. Asymptotic Values of Narrow-Band Longitudinal Pressure Correlation Amplitudes at $\omega \xi/U_c(\omega) = 0$ (from Reference 3).

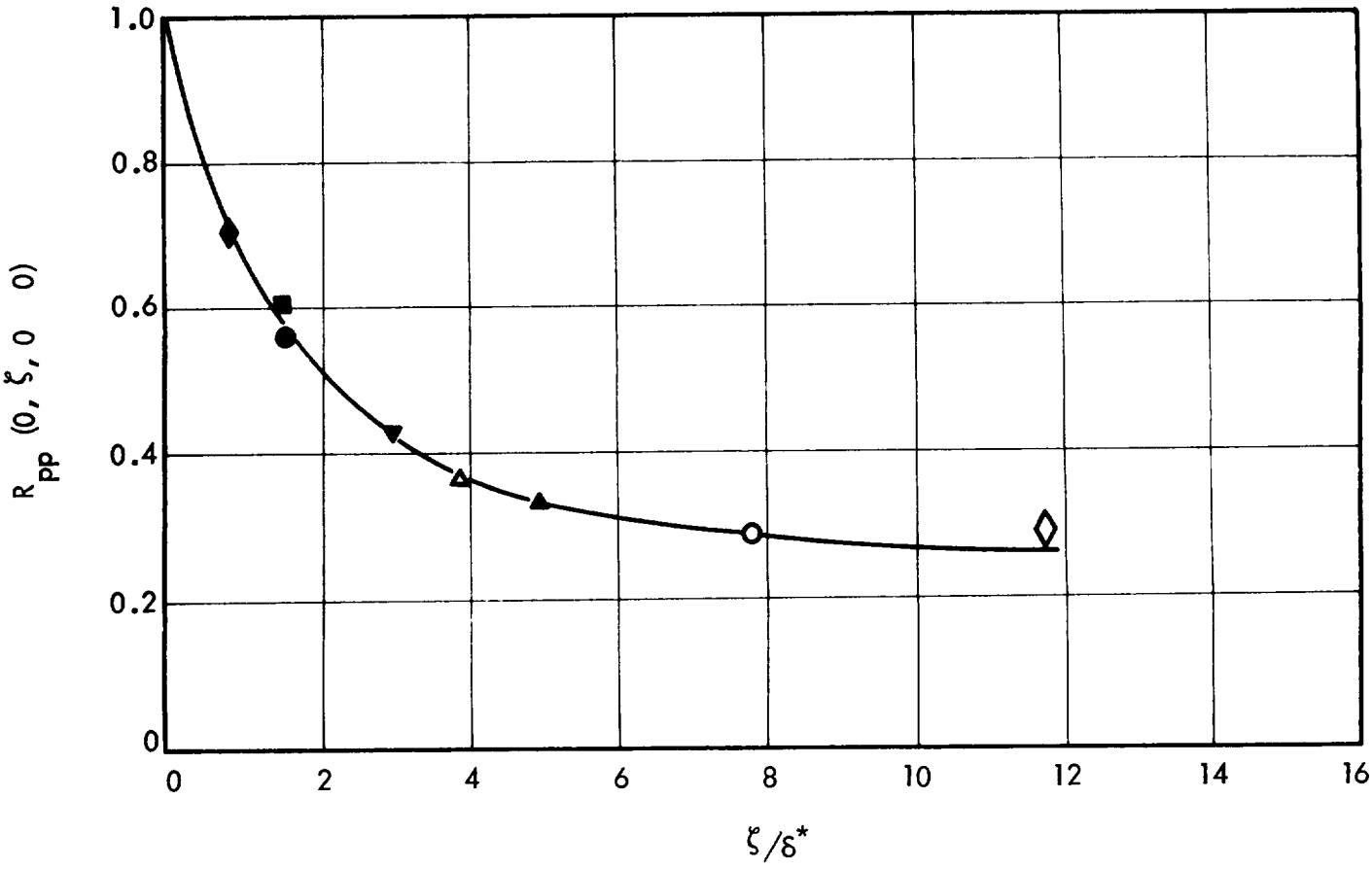

Figure 26. Asymptotic Values of Narrow-Band Lateral Pressure Correlation Amplitudes at $\omega\ \zeta/U_c(\omega) = 0$ (from Reference 3)

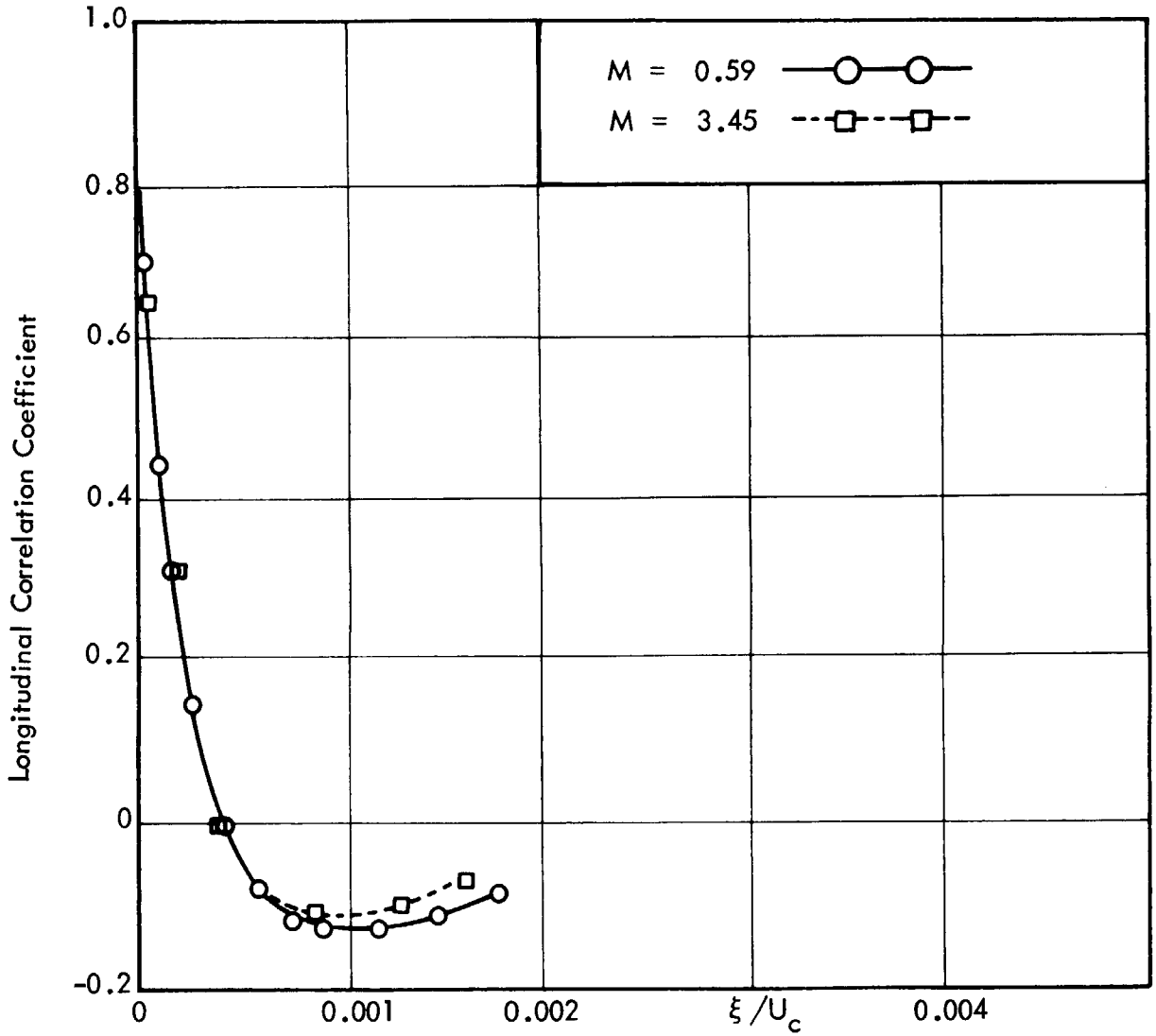

Figure 27. Comparison of Longitudinal Correlation Coefficients (Broadband) at Two Mach Numbers (Extended from Reference 17)

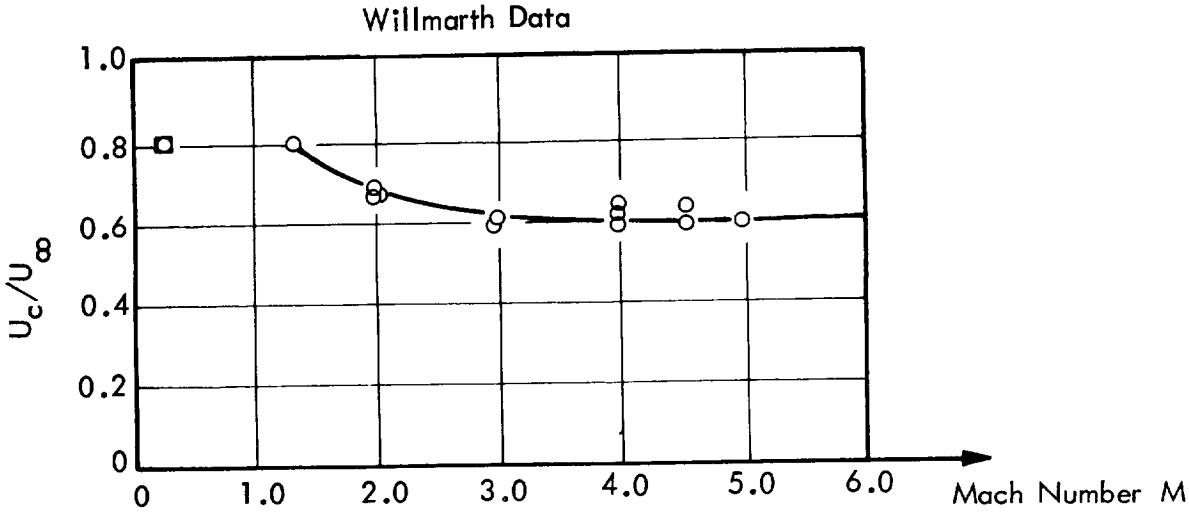

Figure 28. The convection Speed Ratio (from Reference 18)

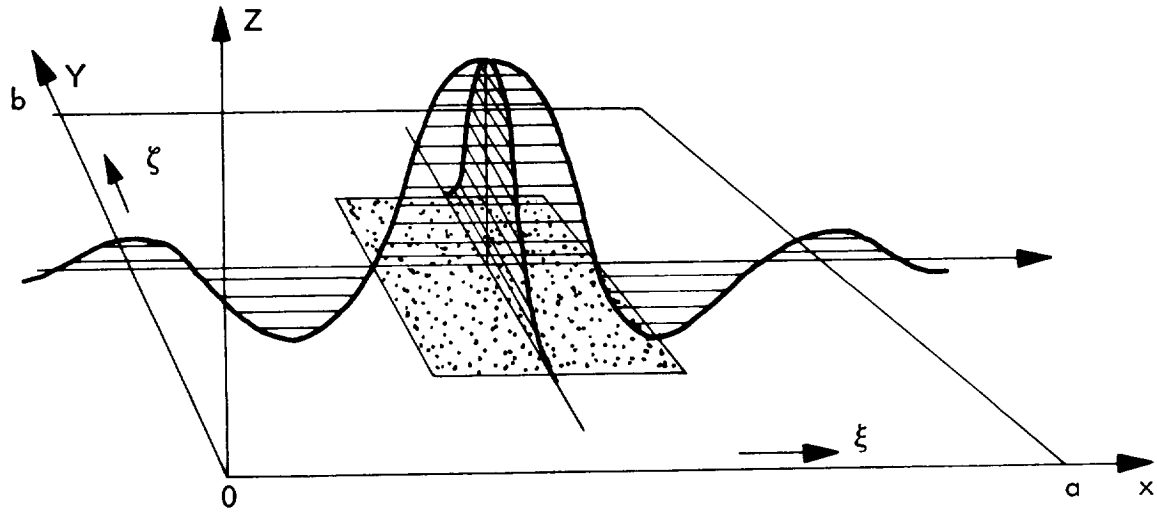

Figure 29. Convected Correlation Pressure Pattern of a Turbulent Boundary Layer

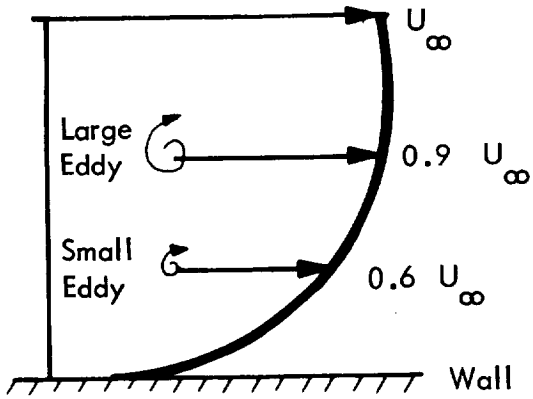

Figure 30. Boundary Layer Profile Showing Eddies and Convection Velocities

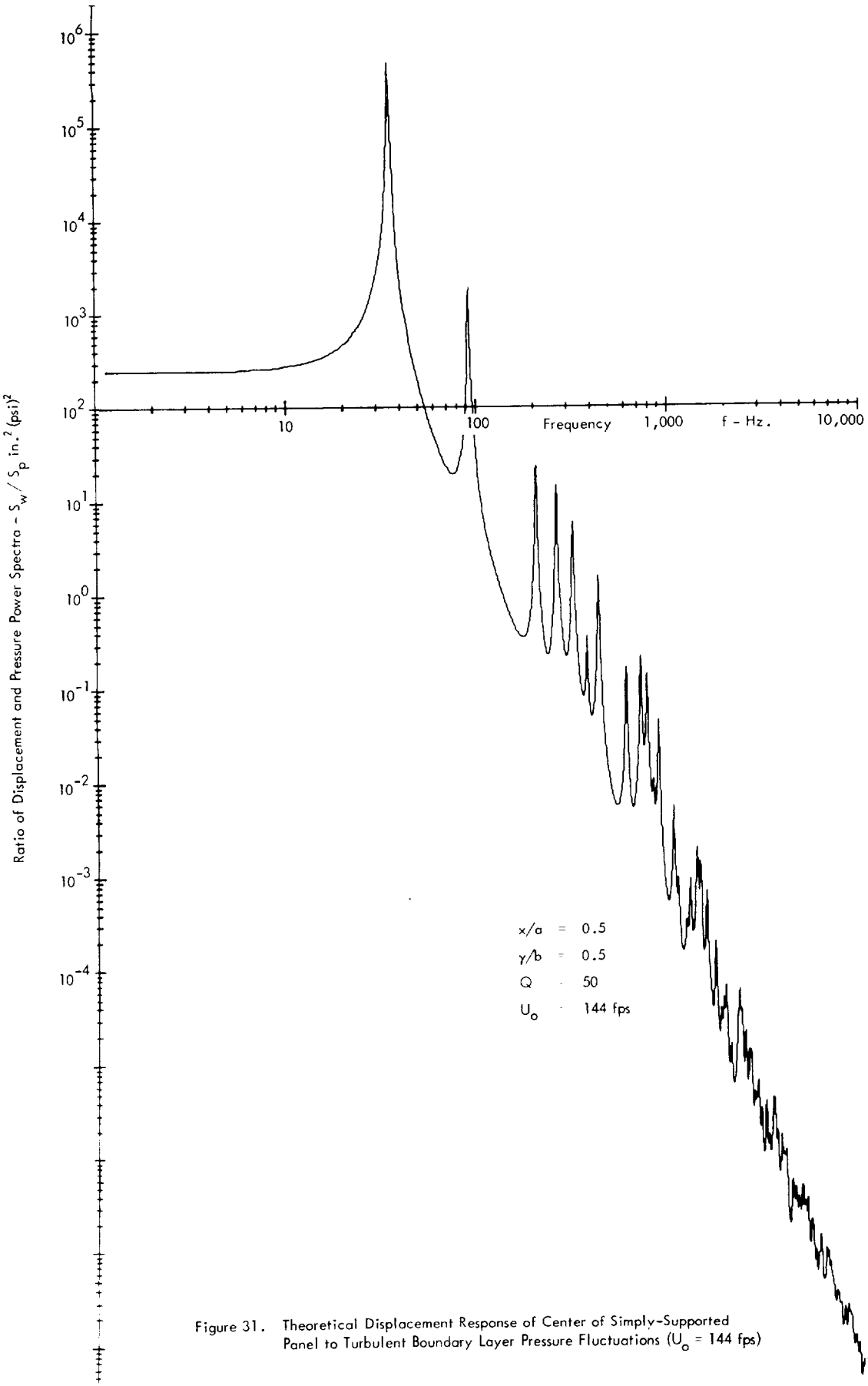

Figure 31. Theoretical Displacement Response of Center of Simply-Supported Panel to Turbulent Boundary Layer Pressure Fluctuations (U_o = 144 fps)

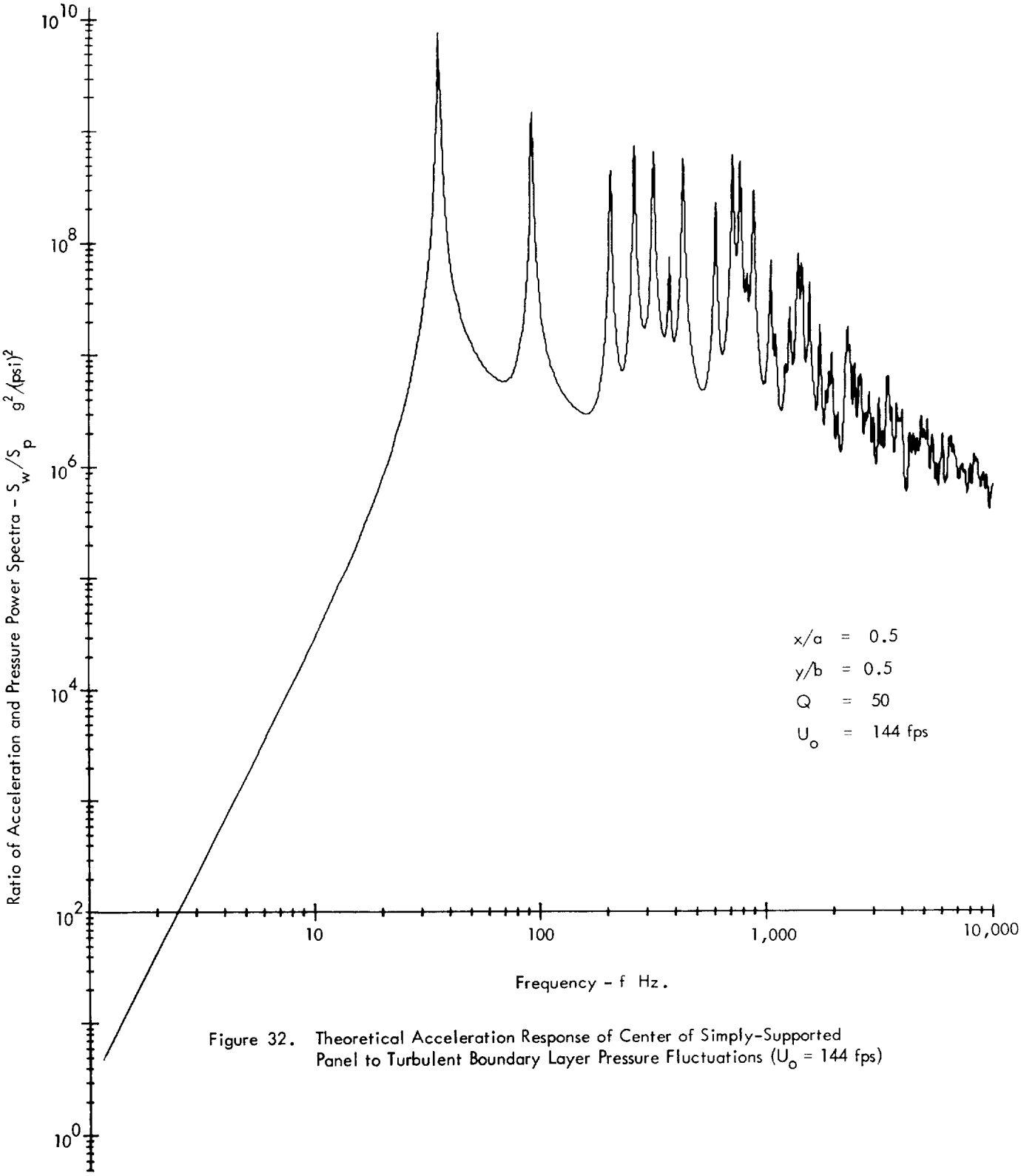

Figure 32. Theoretical Acceleration Response of Center of Simply-Supported Panel to Turbulent Boundary Layer Pressure Fluctuations (U_o = 144 fps)